LBL-22154 c.2
UC-13

Lawrence Berkeley Laboratory
UNIVERSITY OF CALIFORNIA

APPLIED SCIENCE DIVISION

RECEIVED
LAWRENCE
BERKELEY LABORATORY

JUL 31 1987

LIBRARY AND
DOCUMENTS SECTION

FY 1986 Annual Report

ENVIRONMENTAL RESEARCH PROGRAM

May 1987

TWO-WEEK LOAN COPY
This is a Library Circulating Copy
which may be borrowed for two weeks.

APPLIED SCIENCE
DIVISION

Prepared for the U.S. Department of Energy under Contract DE-AC03-76SF00098

LBL-22154 c.2

DISCLAIMER

This document was prepared as an account of work sponsored by the United States Government. While this document is believed to contain correct information, neither the United States Government nor any agency thereof, nor the Regents of the University of California, nor any of their employees, makes any warranty, express or implied, or assumes any legal responsibility for the accuracy, completeness, or usefulness of any information, apparatus, product, or process disclosed, or represents that its use would not infringe privately owned rights. Reference herein to any specific commercial product, process, or service by its trade name, trademark, manufacturer, or otherwise, does not necessarily constitute or imply its endorsement, recommendation, or favoring by the United States Government or any agency thereof, or the Regents of the University of California. The views and opinions of authors expressed herein do not necessarily state or reflect those of the United States Government or any agency thereof or the Regents of the University of California.

LBL-22154

APPLIED SCIENCE DIVISION ANNUAL REPORT

ENVIRONMENTAL RESEARCH PROGRAM

FY 1986

Elton J. Cairns
Head, Applied Science Division
and
Associate Director, LBL

Tihomir Novakov
Program Leader, Environmental Research Program

Applied Science Division
Lawrence Berkeley Laboratory
University of California
Berkeley, California 94720

Prepared for the U.S. Department of Energy under Contract No. DE-AC03-76SF00098

CONTENTS

Introduction 4-1

ATMOSPHERIC AEROSOL RESEARCH

Real-Time Measurements of Aerosol Black Carbon in Urban and Remote Areas
A.D.A. Hansen and T. Novakov 4-2

Spatial and Temporal Variations of Aerosol Sulfate and Trace Elements in a Source-Dominated Urban Environment
M. Bizjak, W.H. Benner, S.G. Chang, A.D.A. Hansen D. Hrčcek, V. Hudnik, and T. Novakov 4-3

Chemical Composition of Aerosol in San Juan, Puerto Rico
W. Reyes, W. Medina, F. Diaz, W.H. Benner, R.L. Dod, and T. Novakov 4-5

Chemical Composition of Summer Fog Water and Interstitial Aerosol in Berkeley
L.A. Gundel, W.H. Benner, A.D.A. Hansen, and T. Novakov 4-6

Fog Chamber Studies of the Nucleation Properties of Soot
W.H. Benner, A.D.A. Hansen, and T. Novakov 4-7

Interaction of NO_2 with Carbon and Alumina Particles
L.A. Gundel, N. Somorjai, and T. Novakov 4-8

Soot-Catalyzed Oxidation of SO_2 in Solution
L.A. Gundel and T. Novakov 4-9

Smoke Characterization from Medium-Scale Fires
R.L. Dod, R.B. Williamson, F. Mowrer, N. Brown, and T. Novakov 4-10

Methane and Carbon Dioxide Increases in the Urban Boundary Layer
K.R. Gurney, A.D.A. Hansen, and T. Novakov 4-11

FLUE GAS CHEMISTRY

Reaction of Nitric Oxide with FE(II) Complexes of SH- Containing Amino Acids
D.K. Liu, D. Littlejohn, and S.G. Chang 4-13

Reaction of Cystine with Hydrogen Sulfide and Sulfite Ions
D.K. Liu and S.G. Chang 4-14

The Reaction of Oxygen with Bisulfite Ion in Aqueous Solution
D. Littlejohn, K.Y. Hu, and S.G. Chang 4-16

The Acid Hydrolysis and Acid Dissociation Constant of Hydroxysulfamic Acid
D. Littlejohn, A.R. Wizansky, and S.G. Chang 4-17

The Photoinduced Reaction of H_2S with CO_2 in the Presence of CdS
D. Littlejohn and S.G. Chang 4-18

COMBUSTION RESEARCH

Controlled Combustion
N.J. Brown, J.A. Cavolowsky, K. Hom, D. Lucas, A.K. Oppenheim, D.A. Rotman, R.F. Sawyer, and H.E. Stewart 4-19

Smoke Emission Factors From Burning Wood and Asphalt as Measured in Medium Scale Experiments
R.B. Williamson, R. Dod, F.W. Mowrer, N.J. Brown, and T. Novakov 4-21

Combustion Chemistry
N.J. Brown, O. Rashed, A.S. Edlin, and D. Lucas 4-23

Combustion Fluid Mechanics
R.K. Cheng, P. Cho, I. Gokalp, J.R. Hertzberg, C.K. Law, M.Z. Pindera, I.G. Shepherd, F. Robben, and L. Talbot 4-26

MEMBRANE BIOENERGETICS

Redox Reactions and Bioenergetic Studies on the Photochemical Conversion of Solar Energy
L. Packer, I. Fry, R Mehlhorn, J. Maguire, S. Belkin R. Giauque, J. D'Souza, W. Nitschmann, E. Hrabeta-Robinson, M. Huflejt, and J. Hrabeta 4-29

ANALYTICAL CHEMISTRY

Impacts of Large Extraterrestrial Bodies and Mass Extinctions
F. Asaro, H.V. Michel, W. Alvarez, and L.W. Alvarez 4-33

ENVIRONMENTAL RESEARCH PROGRAM STAFF

Tihomir Novakov, Program Leader
Nancy Brown, Deputy Program Leader

ATMOSPHERIC AEROSOL RESEARCH

Henry Benner
Mirke Bizjak*
Fernando Diaz*
Raymond Dod
Lara Gundel
Kevin Gurney
Anthony Hansen
Samuel Markowitz
Wallis Medina*
Tihomir Novakov†
Roland Otto
Wanda Reyes*
Hal Rosen*
Richard Schmidt
Nicole Somorjai
Wenzhi Song*
Su Wei-Han*
Linda Wroth

FLUE GAS CHEMISTRY

Shih-Ger Chang
Lawrence Frick
Ke-Yuan Hu*
David Littlejohn
David Liu
Daniel Sigg
Abbey Wizansky

COMBUSTION RESEARCH

James Ang
Steve Beatty
James Bonini
Diana Brehob
Mark Brosmer
Nancy Brown†
John Cavolowsky
Robert Cheng
Peck Cho‡
Danielle DeFontaine
Charles Fleischman
Erica Fono
Stephanie Frolich
Iskander Gokalp*
Ralph Greif
Jean Hertzberg
Kenneth Hom
Wei-Ming Huang
Gary Hubbard
Frank Hurlbut
Antonia Hutchinson
Eileen Javar
Kamal Khayat
Chung Lau‡
Donald Lucas
Richard Martin
Fred Mowrer
Antoinette Nascimento
Antoni Oppenheim
Ahmed Rashed
Ola Rashed
Chang Woo Rhee
Frank Robben
Douglas Rotman
Robert Sawyer
Ian Shepherd§
Pauline Sherman
Horton Stewart§
Lawrence Talbot
Eric Wakahiro
R. Brady Williamson

MEMBRANE BIOENERGETICS

Charles Blanchard
Karen Chin
Ian Fry
John Harte
Eva Hrabeta
Margaret Huflejt
Johanna Lang
John Maguire
Rolf Mehlhorn
Harvey Michaels
Lester Packer†
Richard Schneider

ANALYTICAL CHEMISTRY

Thomas Adelman
Frank Asaro
Robert Giauque
Helen Michel
Amos Newton
Linda Sindelar
Fred Stross*

ADMINISTRATIVE SUPPORT

Gloria Gill
Patti Hannah
Rachelle Edmond

*Participating guest, †Group Leader, ‡University of California Davis, §University of California Berkeley.

ENVIRONMENTAL RESEARCH PROGRAM

INTRODUCTION

The objective of the Environmental Research Program is to understand the formation, transformation, transport, and effects of energy-related pollutants on the environment. This multidisciplinary research program includes fundamental and applied research in physics, chemistry, engineering, and biology, as well as research on the development of advanced methods of measurement and analysis. The Program's Annual Report contains summaries of research performed during FY 1986 in the areas of atmospheric aerosols, flue gas chemistry, combustion, membrane bioenergetics, and analytical chemistry.

The main research interests of the atmospheric aerosol research group concern the chemical processes that occur in haze, clouds, and fogs, and the role of particulate carbon in global climate modification. For their studies, the group developed novel analytical and research methods for characterizing particles, fog, and aerosol species. Aerosol research is performed in the laboratory and in the field. National and international cooperative studies constitute the principal emphasis of the field studies.

The flue gas chemistry research group is investigating the chemical character of pollutants generated by the combustion of fossil fuels to develop new, efficient strategies for pollutant emission control. Current research is directed toward understanding the kinetics and mechanisms of homogeneous and heterogeneous catalysis of the interactions of sulfur dioxide and nitrogen oxides, both among themselves and with other compounds. When this fundamental chemistry is understood, it will be applied to the development of an efficient, cost-effective scrubber for simultaneous desulfurization and denitrification of flue gases.

The combustion research group studies complex combustion processes by acquiring a fundamental understanding of the physical and chemical processes that determine the combustion efficiency, formation, and emissions of species from these processes. Controlled combustion studies have a goal of developing means whereby the zone of chemical activity would be spread out, so that its distribution in space and time could be controlled. The characterization and understanding of turbulence and its relationship to the combustion process are studied in simplified laboratory-scale burners using advanced laser diagnostic techniques. Combustion chemistry studies center on the theoretical understanding of thermal and state-to-state reactions with the purpose of characterizing elementary reactions and developing predictive capabilities. Studies of smoke emissions from fires and their possible effects on climatic change, especially as related to nuclear winter, are an example of the multigroup research effort within the program.

In the membrane bioenergetics group, the study of strongly chemically reactive compounds generated within cells during aerobic metabolism is of particular interest in attempting to understand cellular damage and repair. In particular, active oxygen species (including free radicals) that are generated during the normal life span of cells have been implicated in many processes that result in altered cellular metabolism. The study of free radicals in mitochondrial membranes focuses primarily on oxygen radicals generated by mitochondria (the energy-generating organelles within cells) during respiration and their effects on biological membranes.

One of the main emphases in analytical chemistry and its applications has continued to be in the area of asteroid impacts and mass extinctions. New analytical developments such as the iridium coincidence spectrometer have enabled new analyses to be performed 500 times faster than before. Geochemical and other tests are made to determine if the iridium-rich rocks are of extraterrestrial origin and hence related to impacts. The nature of the sedimentation of the rocks, the worldwide extent of the extinction horizons, and the extent to which the extinctions are related to impacts are also studied.

The short reports that follow describe the program activities in FY 1986. For many of these reports, more detailed papers have been or will be published in appropriate scientific journals.

ATMOSPHERIC AEROSOL RESEARCH

Real-Time Measurements of Aerosol Black Carbon in Urban and Remote Areas*

A.D.A. Hansen and T. Novakov

Aerosol black carbon is a microcrystalline graphitic material, strongly optically absorbing, that is only produced by incomplete combustion. Due to its long residence time and inertness to atmospheric transformation, it is a good tracer for the impact of combustion emissions on an air mass. At LBL we have developed the aethalometer, an instrument that uses an optical measurement on a continuously collecting filter to measure the concentration of aerosol black carbon in real time. In this article, we present highlights of aethalometer measurement programs at various locations.

ACCOMPLISHMENTS DURING FY 1986

Ground-Level Measurements

During March and April 1986, an aethalometer was installed at the N.O.A.A. observatory at Barrow, Alaska. The data were collected on a 6-min basis and averaged over each hour. Aerosol black carbon concentrations ranged from 60 to 400 ng/m^3. Synoptic-scale variations were noted, in which concentrations would increase by a factor of 2 or 3 for 18 to 36 hr in conjunction with changes in meteorological measurements that indicated the passage of a different air mass over the station. Occasional spikes in the data could be correlated to local vehicular activity upwind.

During August 1986, we operated an aethalometer for 10 days in suburban Los Angeles as part of the Carbon Species Measurement Comparison Study. Data were collected and displayed on a 1-minute basis, showing concentrations from 1 to 12 μg/m^3. The concentrations reflected the local traffic activity, being highest during early morning weekday hours and lowest in the 2-5 a.m. period. On a minute-to-minute basis, the effect of trucks in a nearby parking/delivery area could be seen: the black carbon concentration increased from 2.6 to 9.4 μg/m^3 within 2 min when a truck parked 100 m away with its motor idling.

Airborne Measurements

During January 1986 we participated in the aircraft phase of the Western Atlantic Ocean Experiment with an aethalometer on board the N.O.A.A. P-3 aircraft. The instrument cycle was 3 sec; measurements were averaged each minute and then displayed as a function of altitude. Measured concentrations ranged from 20 ng/m^3 at 4-5 km altitude to peaks in excess of 600 ng/m^3 at lower levels (typically 500-1000 m altitude). Relatively little vertical structure was detected apart from a decline in concentration above the boundary layer. Multiplying the mean concentrations by the offshore air fluxes from the coastal study area (from South Carolina to Maine), we estimated an aerosol black carbon export from the continent of 50,000 tonnes per year.

During March and April of 1986, we participated in the Second Arctic Gas and Aerosol Sampling Project with the same installation as above. The Arctic atmosphere is strongly layered, and the black carbon concentrations showed considerable stratification - for example, from 800 ng/m^3 at 1.8 km altitude to 50 ng/m^3 at 3 km altitude on one flight in the vicinity of Barrow, Alaska. Concentrations in excess of 200 ng/m^3 were routinely detected at all altitudes across the entire Western Arctic study region. These concentrations could lead to aerosol optical absorption depths of 0.01 to 0.025, which may result in a perturbation of the solar radiation balance over the region.

PLANNED ACTIVITIES FOR FY 1987

In collaboration with N.O.A.A., an aethalometer will be installed at the South Pole. Preliminary results indicate a black carbon concentration there of between 1 and 10 ng/m^3, permitting a time resolution of 6-12 hr. A multi-channel aethalometer with size-selective inlets is under construction for laboratory and field studies of the size distribution of carbonaceous aerosols, especially in terms of their water nucleation and growth into droplets under humidifying/condensing conditions.

*This work was supported by the National Oceanic and Atmospheric Administration under contract 40 RANR 520248, Coordinating Research Council, and the U.S. Department of Energy under Contract No. DE-AC03-76SF00098.

Spatial and Temporal Variations of Aerosol Sulfate and Trace Elements in a Source-Dominated Urban Environment*

M. Bizjak,[†] W.H. Benner, S.G. Chang, A.D.A. Hansen, D. Hrček,[‡] V. Hudnik,[†] and T. Novakov

Both local and regional sources contribute to the loading of aerosol sulfate in urban environments. Local sources include primary sulfate produced by the oxidation of fuel sulfur to S(VI) during the combustion process, and secondary sulfate produced by oxidation of sulfur dioxide in the urban atmosphere. Regional sulfate is formed by the gradual oxidation of SO_2 released farther upwind. In the United States, most major SO_2 sources are located outside urban areas, and the sulfate is regionally distributed. Results of a field study are described here that demonstrate the formation of aerosol sulfate of local origin by a process faster than the 2-hr time resolution of the sampling.

ACCOMPLISHMENTS DURING FY 1986

The measurements were performed in Ljubljana, Yugoslavia. During the winter heating season, the principal SO_2 source is the burning of coal for space heating in residential boilers and home furnaces. Samples were collected during February and April, 1985, simultaneously at five locations, providing city-wide temporal variations on the concentrations of SO_2, particulate sulfate, carbon, and trace metals (Pb, As, K, V, Mn, and Fe). The highest emissions during winter are in the city center site, where in older buildings coal is burned in individual stoves that are usually stoked in the morning and in the evening. In the outer, newer residential districts, emissions are lower. Locally generated sulfate should exhibit a spatial inhomogeneity similar to that of primary species produced by the combustion of sulfur-containing fuels, especially under stagnant conditions.

During February 19 and 20, the ambient temperature ranged from -14°C to 0°C, the wind speed was always less than 2 m sec^{-1}, and a temperature inversion formed. The data (Fig. 1) show very high SO_2 concentrations with pronounced morning and evening peaks. Peak concentrations decrease from the city center to the suburbs, reflecting the geographical distribution of sources and their patterns of daily fuel use. Similar variations of soot and source

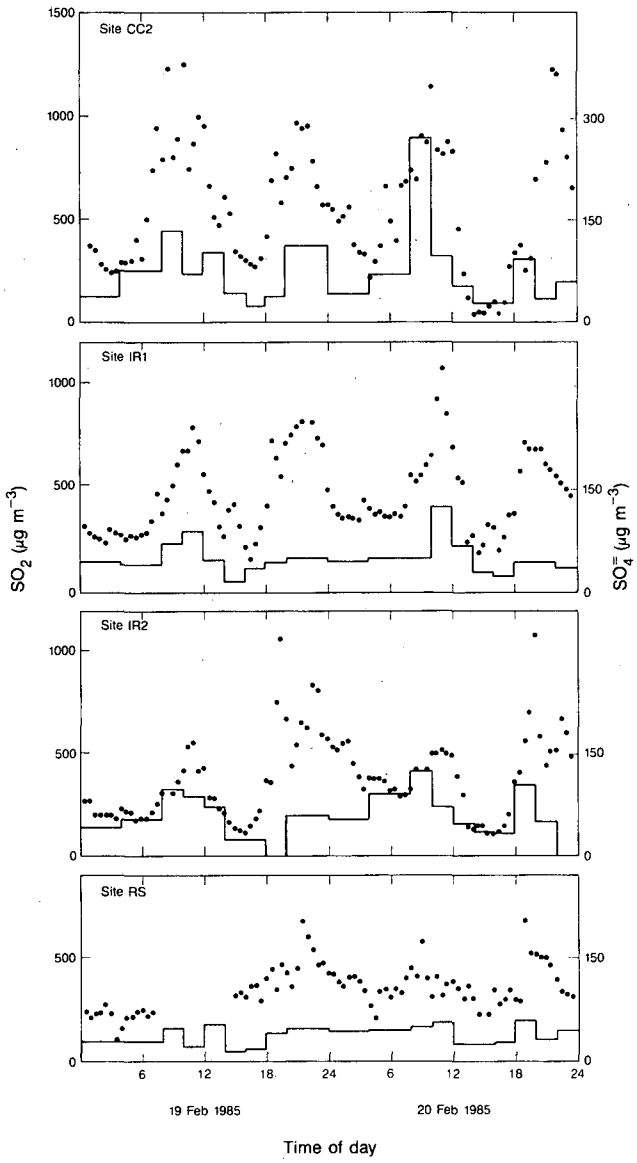

Figure 1. Concentrations of SO_2 and particulate sulfur for February 19 and 20, 1985, at four sites in Ljubljana: CC2 - city center; IR1, IR2 - industrial/residential; RS - residential suburb. (XBL 872-9908)

*The portion of this work done at LBL was supported by the Director, Office of Energy Research, Office of Health and Environmental Research, Physical and Technological Research Division of the U.S. Department of Energy under Contract No. DE-AC03-76SF00098 and by the National Science Foundation under Contract No. ATM 85-13563.

[†]Boris Kidrič Institute of Chemistry, 61115 Ljubljana, Yugoslavia.
[‡]Hydrometeorological Institute of Slovenia, 61000 Ljubljana, Yugoslavia.

tracer elements (K, As, Pb) were observed, confirming the local nature of primary pollutants at each site. The figure also shows variations of sulfate concentrations at the four sites. The spatial inhomogeneity of sulfate concentrations and the similarity with SO_2 and source tracer elements concentration variations indicate local sulfate sources. In Fig. 2, daily variations of relative humidity, ambient temperature, SO_2, sulfate, and particulate carbon at the city center are shown. The lack of direct correspondence between SO_2 and sulfate is seen from the difference in the duration (or width) of their morning peaks. The SO_2 concentration remained essentially constant during the 4-hr period 0800-1200 hr, while the sulfate peaked from 0800-1000 hr. In spite of the persisting large SO_2 concentrations between 1000-1200 hr, sulfate decreased by about a factor of three from the previous 2-hr level. Similarly, the evening SO_2 peak was not accompanied by an equivalent increase in sulfate concentration. Therefore, other factors beside SO_2 must govern the sulfate formation. The relative humidity was about 90% during the night and part of the morning, sharply decreasing after 1000 hr. The fact that the morning sulfate peak occurred during the high-humidity period suggests an aqueous oxidation mechanism, which would be less efficient after 1000 hr than before because of the decreased liquid water content and would therefore produce less sulfate from the same SO_2 concentrations. Because of low ambient temperatures (reaching -13°C at the time of the sulfate concentration peak), these SO_2 oxidation reactions have to proceed in super-cooled water droplets unless much of the oxidation occurs at higher temperatures in plumes.

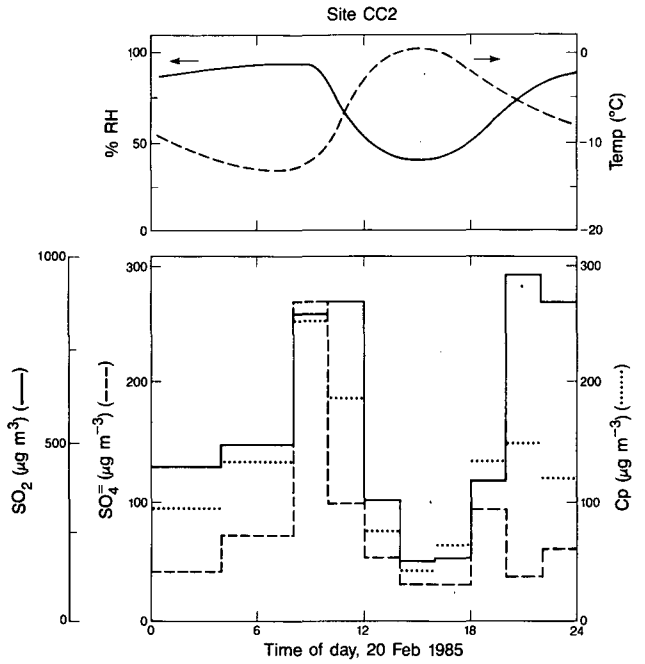

Figure 2. Data for February 20, 1985, taken at the city center site CC2 in Ljubljana. Temperature, humidity, SO_2, particulate carbon (C_p), and sulfate were measured. (XBL 872-9907)

PLANNED ACTIVITIES FOR FY 1987

Measurements of aerosol composition as a function of particle size and fog water composition are planned in cooperation with the Technical University of Vienna and the University of Vienna. Work on the data interpretation will continue.

Chemical Composition of Aerosol in San Juan, Puerto Rico*

W. Reyes,† W. Medina,† F. Diaz,† W.H. Benner, R.L. Dod, and T. Novakov

The objective of this work is the development of a data set to "fingerprint" the aerosol composition of the metropolitan San Juan area. This will be used in conjunction with our planned studies of the aerosol and cloud composition of El Yunque peak to differentiate the species transported over the Atlantic Ocean from locally generated pollutants.

ACCOMPLISHMENTS DURING FY 1986

Aerosol samplers were installed at the Metropolitan University in San Juan. Samples were collected every weekday, from 0800-2000 hours and 2000-0800 hours; on weekends 24-hr samples were gathered. Samples collected on 47-mm Millipore filters were analyzed for trace elements by x-ray fluorescence spectrometry (XRF) and for black carbon by the laser transmission method. Samples on 47-mm quartz filters were analyzed for total particulate carbon and, after water extraction, by ion chromatography (IC). We present preliminary data for three areas - sulfate chemistry, determination of crustal element concentrations, and measurement of ambient particulate mercury.

An insight into sulfate chemistry is provided by the results presented in Fig. 1. Here the ambient concentrations of particulate sulfur, vanadium, and chlorine obtained by XRF are plotted for the entire sampling period. The hatched concentration bars represent daytime samples and the crosshatched bars denote either nighttime or, in some instances, 24-hr samples. It is evident from this figure that the sulfur concentration peaks coincide, especially during April, with those of vanadium. Because vanadium is a tracer for fuel oil combustion, we can conclude that on the days when a sulfur-vanadium correspondence is seen, aerosol sulfur is derived from fuel oil combustion.

It is of interest to note that aerosol chlorine, particularly during the first half of April, is at a minimum when sulfur is at a maximum. This apparent loss of aerosol chloride is an indication of the acidity of the sulfur-bearing particles. Assuming that the source of Na^+ is entirely sea salt, we estimate that the sea salt contributes 26% to ambient sulfate. Based on the $SO_4^=/V$ ratio, we conclude that 46% of non-sea-salt sulfate is derived from fuel oil burning.

The concentrations of Al, Si, Ca, Mn, Fe, and Ti show remarkable remarkable mutual correlations demonstrating their common origin, i.e., soil in the form of suspended dust.

The XRF analyses of ambient filter samples uncovered substantial mercury concentrations, not commonly found in urban environments elsewhere. These concentrations were always higher during the day than at night and did not correlate with any other element. The origin and chemical form of this Hg is not presently known.

PLANNED ACTIVITIES FOR FY 1987

We plan to continue aerosol studies in the San Juan area and are extending the project to aerosol and cloud chemistry studies of El Yunque peak.

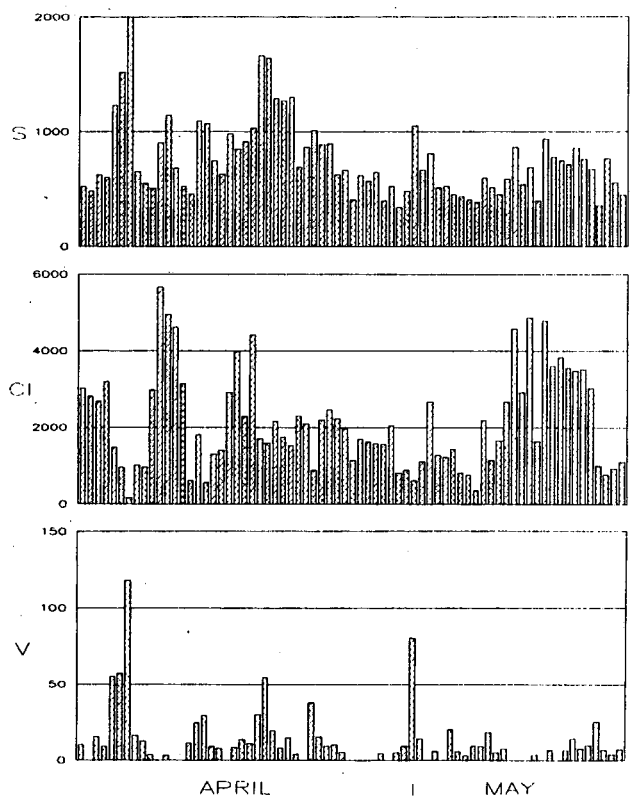

Figure 1. Concentrations in ng/m^3 of S, Cl, and V determined by XRF. (XBL 872-439)

*The portion of this work done at LBL was supported by the Director, Office of Energy Research, Office of Health and Environmental Research, Physical and Technological Research Division of the U.S. Department of Energy under Contract No. DE-AC03-76SF00098 and by the National Science Foundation under Contract No. ATM 85-13563.

†Fundación Educativa Ana G. Méndez, Rio Piedras, Puerto Rico 00928.

Chemical Composition of Summer Fog Water and Interstitial Aerosol in Berkeley*

L.A. Gundel, W.H. Benner, A.D.A. Hansen, and T. Novakov

Combustion-derived pollutants may interact with natural fog and clouds as condensation nuclei, altering the chemical composition of the droplets. In this article, we report on studies of the summertime marine advection fog in the San Francisco Bay Area.

ACCOMPLISHMENTS DURING FY 1986

We sampled fog at LBL using an active mesh collector that collected droplets larger than 5 μm in diameter with >90% efficiency and particles or droplets smaller than 1 μm with negligible efficiency. Fog water drained from the mesh into time-sequenced tubes, and the small particles that penetrated the mesh were collected on a quartz fiber afterfilter. These particles constituted the interstitial component of the total aerosol. An infrared transmissometer continuously monitored the fog density and controlled power to the collector so that it operated only during fog. Another sampler collected the total aerosol on quartz fiber filters sequenced every 4 hr. It preheated the inlet air to evaporate the droplet water and prevent artifact formation of SO_4^{2-} and NO_3^- on wet filters.

With this scheme we obtained three sample types during fog: fog water, interstitial aerosol, and total aerosol. The samples were analyzed by ion chromatography for Na^+, K^+, NH_4^+, Cl^-, NO_3^-, and SO_4^{2-}, and the aerosol samples for black carbon by the laser transmission method.

The liquid water content of the fog ranged from 17 to 120 $\mu l/m^3$ of air, integrated over each event; the pH ranged from 3.4 to 6.3 with a median of 4.0.

Analysis of the fog water from 13 episodes (Fig. 1) showed that the major components of sea salt, Na^+ and Cl^-, were the most abundant species, followed by NH_4^+ and SO_4^{2-}. About 10% of the SO_4^{2-} can be attributed to sea salt. Concentrations of NO_3^- and K^+ were lower than those of the other ions. The sum of the concentrations of the cations (including H^+) equalled the sum of the concentrations of the anions. Organic acids and divalent cations such as Ca^{++} and Mg^{++} contributed little to the ionic balance.

Sulfate and ammonium ions dominated the interstitial particle extract. The most abundant ions in the total aerosol were SO_4^{2-} and Na^+. Ideally the total aerosol collected during fog should equal the sum of all species in fog water and in the interstitial particles. Our results show less than expected amounts of NH_4^+, NO_3^-, and Cl^- but very close to expected amounts of Na^+ and K^+, which are not volatile. Losses of NH_4^+, Cl^-, and NO_3^- were 75, 53, and 48% respectively. The interstitial particles also lost some Cl^- and NH_4^+. The heating necessary to evaporate the fog water probably caused the loss of the volatile compounds NH_4Cl, NH_4NO_3, and HCl from the particles during sampling.

During fog episodes the black carbon concentration averaged 0.63 $\mu g/m^3$, with 73% of this appearing in the interstitial particles. This means that at most 27% of the black carbon, by mass, acted as condensation nuclei.

PLANNED ACTIVITIES FOR FY 1987

We have extended these studies to include radiation fog in California and orographic clouds in Puerto Rico. A dual-channel aethalometer will provide real-time information on black carbon concentration in fog droplets and interstitial particles.

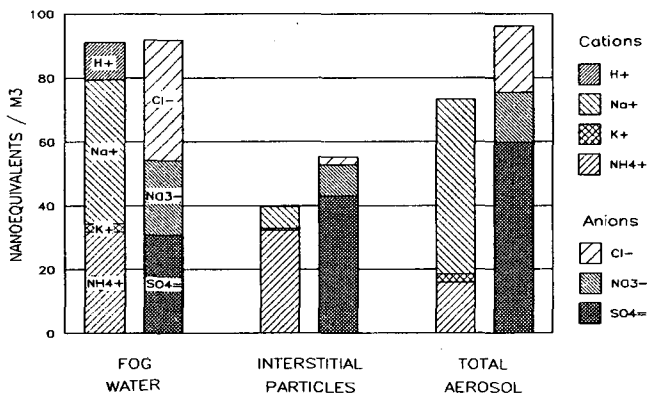

Figure 1. Composition of San Francisco Bay Area fog in nanoequivalents per m^3 for fog water, interstitial particles, and total aerosol. (XBL 871-377)

*This work was supported by the Director, Office of Energy Research, Office of Health and Environmental Research, Physical and Technological Research Division of the U.S. Department of Energy, under Contract No. DE-AC03-76SF00098 and by the National Science Foundation under Contract No. ATM 85-13563.

Fog Chamber Studies of the Nucleation Properties of Soot*

W.H. Benner, A.D.A. Hansen, and T. Novakov

Heterogeneous chemical reactions in the troposphere may lead to the formation of acidic fogs and clouds. Because fog and cloud droplets form by the condensation of water onto nucleation centers (air ions or aerosol particles), changes in the number concentration and the composition of the particles will significantly affect the dynamics of the condensation-evaporation process. In field studies we have observed that aerosol sulfate is related to the soot particle concentration. To study the effects of combustion products (SO_2, soot, primary oxidants) on fog formation and fog chemistry, we have constructed a laboratory fog chamber.

ACCOMPLISHMENTS DURING FY 1986

Construction of the fog chamber (Fig. 1) was completed this year. In this chamber (20 cm × 1.5 m tall), a prehumidified sample of propane combustion products is drawn into the bottom of the chamber where it mixes with cold dilution air. Supersaturation occurs and water condenses onto soot particles. A 2-channel aethalometer is used to collect samples of fog at the top of the chamber; the samples may be used for chemical analysis of the particles. One channel of the aethalometer is preceded by a fog separator that excludes droplets and allows only the interstitial aerosol to penetrate. The other channel is preceded by a heated tube that evaporates the fog and permits detection of total soot

The effect of soot particle composition on fog nucleation was studied by introducing various amounts of SO_2 into the propane fuel. S/propane (wt/wt) was varied between 0 and 2.5%. Typical results for S/propane = 2.5% are shown in Fig. 2. Without added SO_2 about 15% of the total soot is incorporated into droplets; when SO_2 is added into the fuel, the percentage of soot in droplets increased to ~90 and a decrease in the total soot concentration at the top of the chamber is observed.

These effects of fuel S may be due to the formation of hygroscopic particles. Fresh soot particles are nominally hygrophobic but become coated with $SO_4^=$

*This work was supported by the Director, Office of Energy Research, Office of Health and Environmental Research, Physical and Technological Research Division of the U.S. Department of Energy under Contract No. DE-AC03-76SF00098 and by the National Science Foundation under Contract ATM 85-13563.

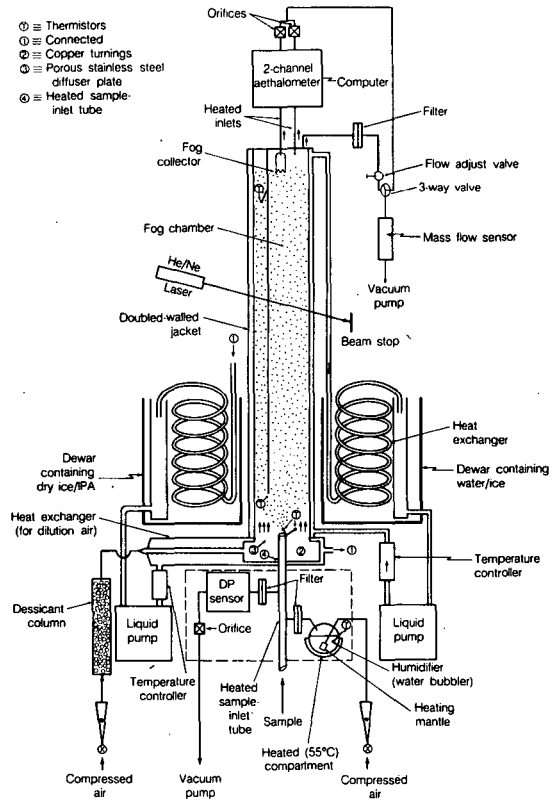

Figure 1. Fog chamber and associated equipment. (XBL 8612-9269)

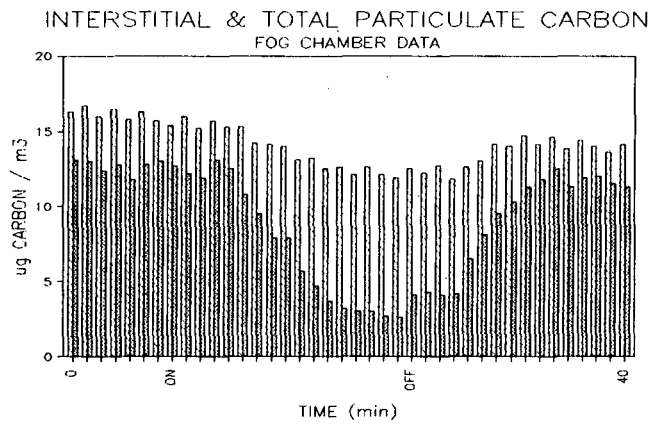

Figure 2. Changes in the nucleation of fog by soot particles due to the addition of SO_2 into the propane fuel. Darkest bars show interstitial soot particle concentration and striped bars show total soot particle concentration. (XBL 871-151)

(its presence verified by analysis) when SO_2 is added to the fuel. This coating converts them to hygroscopic particles that nucleate fog more readily. The presence of $SO_4^=$ also causes the size of the droplets to grow. The large droplets can no longer be carried to the top of the chamber because their settling velocities are greater than the upward air velocity. This effect decreases the detected soot particle concentration by raining out some of the particles when SO_2 is added to the fuel.

PLANNED ACTIVITIES FOR FY 1987

These results show the strong influence of fuel and source aerosol composition on the water nucleation and ultimate atmospheric lifetime of soot particles. We will continue these studies and aim to separate physical from chemical effects. The laboratory work will be paralleled by field sampling of fog and aerosols.

Interaction of NO_2 with Carbon and Alumina Particles*

L.A. Gundel, N. Somorjai, and T. Novakov

Nitric acid is an important component of acid deposition. In this work we studied the production of NO_2^- and NO_3^- by the interaction of NO_2 gas with carbon and alumina particles and water.

ACCOMPLISHMENTS DURING FY 1986

Mixtures of ~ 5 ppm NO_2 in air were passed at 1 liter/min through impingers containing alumina or activated carbon particles dispersed among glass beads. After 10 min the 20-mg sample of particles was extracted with water for determination of NO_2^- and NO_3^- by ion chromatography. In some experiments we added humidified air upstream of the reaction vessel. To investigate reactions in water, the impinger contained slurries of 10-mg particles in 10 ml water.

Alumina, glass beads, and liquid water all trapped some NO_2 from the gas phase, as shown in Fig. 1. Analysis of the extract or water alone showed approximately equal concentrations of NO_2^- and NO_3^-. This corresponds to reactive dissolution of NO_2 according to:

$$2NO_2 + H_2O \rightarrow HNO_2 + H^+ + NO_3^- \quad (1)$$

When carbon was present, Fig. 1 shows that NO was observed downstream of the reaction vessel due to the reduction:

$$NO_2 + C_x \rightarrow NO + C_xO \quad (2)$$

Further adsorption of NO_2 at the C_xO sites led to the appearance of NO_3^- in the water extract:

$$NO_2 + C_xO \rightarrow C_xO \cdot NO_2 \quad (3)$$

$$NO_2 + C_xO \cdot NO_2 + H_2O \rightarrow$$

$$2H^+ + 2NO_3^- + C_x. \quad (4)$$

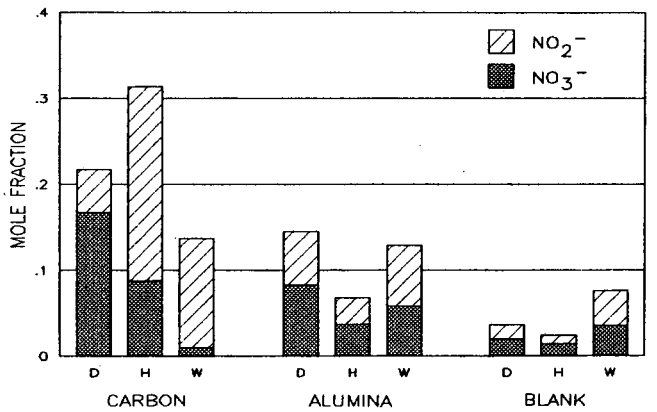

Figure 1. NO_2^- and NO_3^- from interactions of NO_2 gas in air with carbon and alumina particles, under dry (D), humid (H), or wet slurry (W) conditions. The results are expressed as mole fractions of total $NO_2(g)$ entering the reaction vessel. (XBL 871-376)

*This work was supported by the Director, Office of Energy Research, Office of Health and Environmental Research, Physical and Technological Research Division of the U.S. Department of Energy, under Contract No. DE-AC03-76SF00098 and by the National Science Foundation under Contract No. ATM 85-13563.

In the presence of water vapor or liquid, the NO reacted with NO_2 to form HNO_2:

$$NO + NO_2 \rightarrow 2HNO_2. \quad (5)$$

This process dominated surface oxidation of NO_2 when water vapor was available and led to high NO_2^- concentrations on the wet carbon particles. It was more effective than the C_xO mechanism (reactions (3) and (4)) when water was present.

PLANNED ACTIVITIES FOR FY 1987

We plan to continue this work with carbon, combustion soot, urban particulate matter, and slurries of typical fog water composition.

Soot-Catalyzed Oxidation of SO_2 in Solution*

L.A. Gundel and T. Novakov

The oxidation of dissolved SO_2 occurs at sites on carbon particles where oxygen is held in a surface complex, C_xO_2. The range of oxidation rates displayed by different carbons depends on their abilities to form the surface complex C_xO_2. Heat treatment in an inert atmosphere before exposure to air at room temperature enhances this ability and hence increases the reaction rate. The rate of oxidation also depends on the rate of adsorption of two S(IV) ions to the active site, and the rate of dissociation of this complex to two $SO_4^=$ ions and an empty C_x site. At low [S(IV)] concentrations, the overall rate has second-order dependence on [S(IV)], changing to first and then zero order as the [S(IV)] increases. At low concentrations, the rate is controlled by the adsorption steps; at high concentrations the surface is saturated, and the dissociation of the products controls the reaction rate.

ACCOMPLISHMENTS DURING FY 1986

We measured the effect of heat treatment of the particles on the reaction rate and reaction order with respect to [S(IV)] for two commercial carbons, Norit RB 1 and Nuchar SN. The reaction order for Nuchar varied only from 0.55 to 0.59 with heat treatment over the S(IV) concentration range from 1×10^{-5} to 1×10^{-3} M, but the overall rate increased by a factor of about 6. Heat treatment of RB 1 increased its reaction order from 0.59 to 1.25; the rate increased by 13 at initial [S(IV)] = 4×10^{-4} M. These data are consistent with the mechanism outlined above, and they indicate that heat treatment had different effects on the two carbons. For Nuchar the rates of S(IV) adsorption steps were unchanged but the number of active C_xO_2 sites grew. This increased the rate without altering the reaction order with respect to [S(IV)]. For RB 1, the faster carbon, both the number of C_xO_2 sites and the S(IV) adsorption rate increased with heat treatment.

PLANNED ACTIVITIES FOR FY 1986

We will investigate the oxidation of S(IV) by carbons that have been exposed to NO_2.

*This work was supported by the Director, Office of Energy Research, Office of Health and Environmental Research, Physical and Technological Research Division of the U.S. Department of Energy, under Contract No. DE-AC03-76SF00098 and by the National Science Foundation under Contract No. ATM 85-13563.

Smoke Characterization from Medium-Scale Fires*

R.L. Dod, R.B. Williamson, F. Mowrer, N. Brown, and T. Novakov

Evaluation of the potential significance of a "nuclear winter" produced by smoke from post-nuclear exchange fires depends largely upon the quantity of smoke generated, its distribution in the atmosphere, and its optical characteristics. We have made measurements of the amount and composition of smoke emitted from medium-scale (0.3-1.3 MW peak) fires of exemplar urban building materials under both open and restricted ventilation conditions. This information can be used to increase the accuracy of the predictions of the effects of "nuclear winter."

ACCOMPLISHMENTS DURING FY 1986

The fuels used in our experiments to date are softwood (both solid wood and plywood) and asphalt roofing material. Smoke samples were collected by filtration and with a cascade impactor to determine the aerodynamic size distribution. The particles were weighed to determine mass and analyzed for total carbon by combustion; the carbon was differentiated into black and organic carbon by thermal evolved gas analysis.

Six experiments were conducted with Douglas fir plywood sheets (6 ft by 4 ft) in parallel plate configuration. Five of these fires were used to establish the degree of reproducibility as well as to determine emission factors for 5-ply, 1/2-in. CDX plywood under well-ventilated conditions. Experiments 3 through 5 were very similar in fuel and in details of combustion configuration. As can be seen from Table 1, the reproducibility was excellent. Experiment number 10 was conducted with 3-ply plywood, and showed significantly less emissions. Use of solid Douglas fir dimension lumber (as a crib) showed even lower emissions when burned under well-ventilated conditions (experiment 11), indicating that substantial amounts of the smoke produced were either from the glue or an artifact of the laminated construction of the plywood. In addition, solid wood cribs were burned under ventilation-restricted conditions (experiments 12 and 13), which led to greatly increased emissions as well as a shift in particle aerodynamic diameter to larger size ranges. Asphalt roofing material burned under well-ventilated conditions (experiment 9) produced smoke emissions much larger than those observed for wood products under any tested conditions.

Table 1. Smoke emissions as percent of fuel mass consumed.

	Emission Factors (%)			
Experiment	Non-Carbon	Black Carbon	Organic Carbon	Total
1 - plywood	-	.13	.03	-
2 - plywood	.00	.17	.06	.24
3 - plywood	.02	.12	.04	.18
4 - plywood	.03	.13	.04	.20
5 - plywood	.01	.13	.05	.20
9 - asphalt roofing	2.05	10.03	1.85	13.94
10 - plywood	.04	.09	.01	.14
11 - wood crib in open	.01	.05	.02	.09
12 - 3 wood cribs in room	.53	1.12	.29	1.93
13 - 3 wood cribs in room	.31	2.66	.54	3.51

*This work was supported by the Defense Nuclear Agency through the U.S. Department of Energy under Contract No. DE-AC03-76SF00098.

The composition of smoke particles was similar for all experiments as determined by measurements of total mass as well as organic and black carbon. The dominant component in all samples was black carbon as shown in Table 1. In addition, all well-ventilated fires exhibited the greatest mass concentration of particles to be in aerodynamic sizes below 0.3 μm. A typical mass histogram is shown in Fig. 1. Wood burned under restricted ventilation conditions produced peak mass in such a histogram in particle sizes between 1 and 2 μm, undoubtedly due to the burning of fuel pyrolysates at a distance significantly removed from the primary fire.

PLANNED ACTIVITIES FOR FY 1987

Further experiments are in progress to extend the study to other fuels (e.g., polyurethane foam, liquid hydrocarbons) and to study the effect of scale with significantly larger and/or smaller fires.

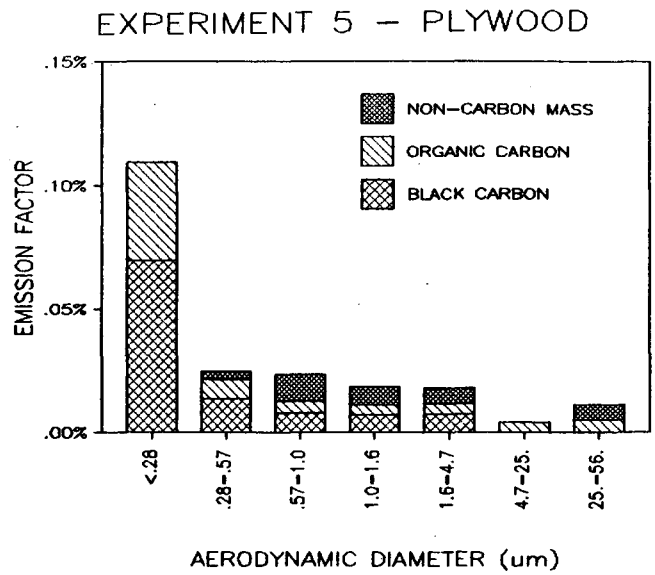

Figure 1. Typical smoke emissions as percent of fuel consumed. (XBL 871-150)

Methane and Carbon Dioxide Increases in the Urban Boundary Layer*

K.R. Gurney,[†] *A.D.A. Hansen, and T. Novakov*

The transparency of the atmosphere in the 8- to 10-μm infrared region is affected strongly by the concentration of certain infrared absorbing gases. Energy-related activities may increase these concentrations, altering the radiation balance and leading to atmospheric heating. On a global scale, this is referred to as the "greenhouse effect." In this work we studied concentration increases at a local scale, within the urban boundary layer.

ACCOMPLISHMENTS DURING FY 1986

We set up an FTIR spectrometer with a solar tracking coelostat to measure the whole-column atmospheric infrared absorbance spectrum, using the sun as a source. Spectral lines due to specific gases were identified: those for carbon dioxide and methane were fit to collision-broadened Lorentzian line shapes. Measurements were made close to solar noon on 35 days over a several-month period. After correcting for path length variations, these measurements yield a total atmospheric column absorbance for CO_2 and CH_4. The lowest values of these column absorbances were observed on clear windy days, corresponding to the total column of these two gases under unpolluted conditions. Variations of up to 8% may be expected due to seasonal effects; however, under polluted conditions we observed large increases in the infrared absorbance. The maximum carbon dioxide absorbance was 1.48 times its lowest value; for methane, the greatest increase was 42%. These increases must be due to local contributions within the boundary layer. Assuming a range of depths for the boundary layer, we may calculate the concentration increase factors necessary to account for the increased strengths of the spectral absorbances. For both gases, a local doubling is required.

*This work was funded by Project Development Funds through the U.S. Department of Energy under Contract No. DE-AC03-76SF00098.

[†]Present address: Mailstop L-524, Lawrence Livermore National Laboratory, P.O. Box 808, Livermore, CA 94550.

Increases of this magnitude have been indicated by ground-level sampling and chemical analysis; however, the spectroscopic technique gives the result, independent of the actual boundary layer depth, in the form of an infrared absorbance as required for calculations of the perturbation of radiative transfer in the urban environment.

PLANNED ACTIVITIES FOR FY 1987

This project has been concluded.

Reaction of Nitric Oxide with Fe(II) Complexes of SH-Containing Amino Acids*

D.K. Liu, D. Littlejohn and S.G. Chang

We have recently reported a flue gas simultaneous desulfurization and denitrification process using an alkaline ferrous cysteine solution.[1] Compared to the ferrous chelates such as Fe^{2+}(EDTA) developed by the Japanese, the ferrous cysteine system produces little or no dithionate and nitrogen-sulfur compounds. Other advantages include the ability of cysteine to reduce Fe^{3+} to Fe^{2+} and that the oxidation product cystine can be conveniently converted back to cysteine. Our goal has since been to find Fe(II) complexes of other SH-containing amino acids/peptides which are more resistant than ferrous cysteine towards oxidation by the residual oxygen in flue gas.

ACCOMPLISHMENTS DURING FY 1986

We have discovered that basic solutions of Fe(II) complexes of three cysteine derivatives, penicillamine (β,β'-dimethylcysteine), N-acetylcysteine and glutathione (γ-glutamylcysteinylglycine) can effectively remove NO from a simulated flue gas.[2] The experiments were carried out at 55°C and between pH 6.8 - 12.0 by bubbling a gaseous mixture of NO(P_{NO} = 500 ppm), O_2 (0% or 4%) and N_2 (balance) into an absorber containing an aqueous solution of ferrous salt (0.01 M) and cysteine or cysteine derivative (0.04 M). The results are shown in Figures 1 and 2. When oxygen is absent from the simulated flue gas, ferrous cysteine is more effective in absorbing NO than the corresponding penicillamine and N-acetylcysteine (Fig. 1). The presence of 4% O_2 in the simulated flue gas significantly reduces the NO absorption capacity of all ferrous amino acid complexes, with ferrous cysteine being the most adversely affected (Fig.2). While the NO absorption capacity of ferrous cysteine is fairly pH independent, the ferrous pencillamine, N-acetylcysteine and glutathione systems more efficient as the solutions become more acidic, up to pH ~ 5. It is important to point out that while the effectiveness for NO absorption for the ferrous amino acid complexes in the presence of 4% O_2 follows the order Fe(glutathione) > Fe(penicillamine) > Fe(N-acetylcysteine) ≥ Fe(cysteine), the rate of NO absorption follows a reversed order.

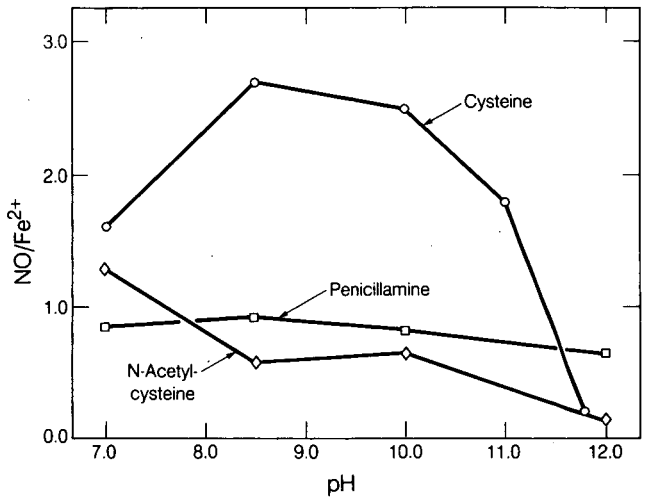

Figure 1. Absorption of NO by ferrous cysteine/cysteine derivatives in the absence of O_2. (XBL 8612-10205)

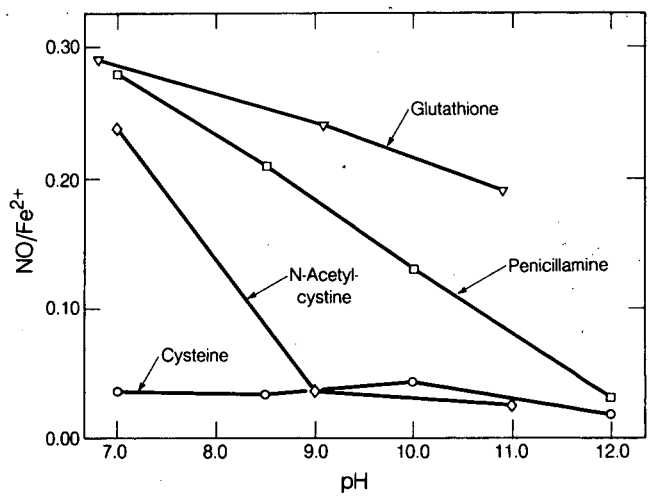

Figure 2. Absorption of NO by ferrous cysteine/cysteine derivatives in the presence of 4% O_2. (XBL 8612-10204)

*This work was supported by the Assistant Secretary for Fossil Energy, Office of Coal Utilization Systems, U.S. Department of Energy under Contract No. DE-AC03-76SF00098 through the Pittsburgh Energy Technology Center, Pittsburgh, PA.

The fate of the absorbed NO has been studied in some detail. In the ferrous cysteine system, part of the NO absorbed was complexed reversibly to the metal chelate and isolated as a solid at pH $\sim$ 7 and in the absence of O_2.[1] Otherwise all the NO was reduced to N_2O and N_2 in the gas phase and/or converted to small amount ($\sim$ 6%) of NO_2^- solution. However, we were unable to detect by IR an analogous nitrosyl complex for ferrous pencillamine. In the ferrous glutathione system, all of the absorbed NO was converted to a mixture of NO_2^- (> 90%) and NO_3^- at pH > 7. When the absorption was carried out at pH $\sim$ 5, < 10% NO_2^-/NO_3^- and no N_2O/N_2 were detected, which suggested the formation of an iron nitrosyl complex. In all cases, iron (II)/(III) hydroxide and an oxidized (dimeric) form of the amino acids were formed at pH > 9. The different NO-derived products imply different mechanisms are involved with various ferrous amino acid complexes.

PLANNED ACTIVITIES FOR FY 1987

We plan to investigate in greater detail the kinetics and mechanisms of the reaction between the above ferrous amino acid complexes with NO. In addition, we plan to test these additives in a spray drying system for the simultaneous removal of NO_x and SO_2 from flue gas.

REFERENCES

1. Tu, M.D., and Chang, S.G. (1987), "Chemistry of a Flue Gas Combined NO_x and SO_2 Scrubber Employing Ferrous Cysteine Additives," *AIChE Environ. Progr.*, in press.
2. Liu, D.K., Griffiths, E.A., Littlejohn, D. and Chang, S.G. (1986), "A Process for the Combined Removal of SO_2 and NO_x from Flue Gas," U.S. patent pending.

Reaction of Cystine with Hydrogen Sulfide and Sulfite Ions*

D.K. Liu and S.G. Chang

It has recently been discovered in our laboratory that an alkaline solution containing ferrous cysteine can be employed as an additive in both wet and spray drying systems to enhance the removal efficiencies of NO_x and SO_2 from flue gas.[1,2] In this process, cysteine is oxidized to cystine by residual oxygen in flue gas, and this reaction is catalyzed by the presence of ferrous ions. Existing methods for the conversion cystine to cysteine include electro- and chemical reductions. However, these methods require the consumption of electric energy or relatively expensive chemical reagents. Therefore, a cost-effective process to reduce cystine back to cysteine for recycling in the scrubber system is needed.

*This work was supported by the Assistant Secretary for Fossil Energy, Office of Coal Utilization Systems, U.S. Department of Energy under Contract No. DE-AC03-76SF00098 through the Pittsburgh Energy Technology Center, Pittsburgh, PA.

ACCOMPLISHMENTS DURING FY 1986

Conversion of Cystine to Cysteine by Hydrogen Sulfide and Sulfite Ions

We have demonstrated that the regeneration of cysteine (CySH) from cystine (CySSCy) can be accomplished by treatment of a basic solution of CySSCy with H_2S (or sulfide) and SO_2 (or sulfite/bisulfite), either simultaneously or in sequence.[2,3] The mechanism involved can be represented by the following equations:

$$\mathrm{CySSCy} + \mathrm{HS}^- \underset{k_{-1}}{\overset{k_1}{\rightleftharpoons}} \mathrm{CySH} + \mathrm{CySS}^- \qquad (1)$$

$$\mathrm{CySS}^- + \mathrm{HS}^- \underset{k_{-2}}{\overset{k_2}{\rightleftharpoons}} \mathrm{CySH} + \mathrm{S_2}^{2-} \qquad (2)$$

$$\mathrm{CySS}^- + \mathrm{SO_3}^{2-} \rightleftharpoons \mathrm{CyS}^- + \mathrm{S_2O_3}^{2-} \qquad (3)$$

$$\mathrm{CySSCy} + \mathrm{SO_3}^{2-} \rightleftharpoons \mathrm{CyS}^- + \mathrm{CySSO_3}^- \qquad (4)$$

$$CySSO_3^- + HS^- \rightleftarrows CySH + S_2O_3^{2-} \quad (5)$$

where $CySS^-$ and $CySSO_3^-$ represent S-thiocysteine and cysteine sulfonate, respectively.

The results for the regeneration of CySH from CySSCy are presented in Table 1. When a cystine solution at pH 10 and 60°C was allowed to react first with two equivalents of Na_2S, followed by three equivalents of Na_2SO_3 (Method I), the reaction reached equilibrium in ~ 30 min with 59% CySH, 17% $CySSO_3^-$ and 15% CySSCy in the equilibrium mixture. The simultaneous addition of Na_2S and Na_2SO_3 to a cystine solution (Method II) under the same conditions yielded less CySH (36%). The best result obtained was from the reaction of cystine first with H_2S and then SO_2 (Method III). In this case, a 90% yield of CySH was attained. When H_2S and SO_2 were applied simultaneously under the same reaction conditions (Method IV a), CySH was obtained in 85% yield. Finally, raising the reaction temperature to 80°C (Method IV b) or increasing the pH to 12 (Method IV c) had little effect on the equilibrium concentration of CySH.

Kinetic Study of the Reaction Between Cystine and Sulfide in Alkaline Solutions

The reaction between cystine (CySSCy) and hydrogen sulfide ion (HS^-) in alkaline solutions yields cysteine (CySH), S-thiocysteine ($CySS^-$) and disulfide (S_2^{2-}) in two reversible steps represented by equations (1) and (2) above. We have undertaken a detailed kinetic study of these two reactions by a combination of UV-vis spectroscopy and amino acid analysis.[4] The equilibrium constants K_1 and K_2 have been determined, and the results are listed in Table 2. The fact that the apparent equilibrium constants vary with pH can be explained by the presence of different charge forms of CySSCy, CySH, $CySS^-$ and HS^- at different pH.

Table 1. The conversion of cystine to cysteine under various conditions.

Method	CySH %	$CySSO_3^-$ %	CySSCy %
I	59	17	15
II	36	3	58
III	90	5	4
IVa	85	8	6
IVb	84	10	6
IVc	84	6	5

Table 2. Equilibrium constants of Eq. 1 and Eq. 2 at various pH at 25°C.

pH	K_1	K_2
8.0	0.16	0.21
9.0	0.49	0.06
10.0	0.65	0.05
11.0	0.87	0.04
12.0	~ 4.2	0.02

The rate constants k_1, k_{-1}, k_2 and k_{-2} for Eqs. (1) and (2) have been determined using the following equation:

$$\frac{1}{k_i} = \frac{k_{-1}[CySH]_o}{k_1 k_2 [HS^-]_o^2} + \frac{1}{k_1[HS^-]_o} \quad (6)$$

where k_i represents the pseudo first-order initial-rate constant, and $[CySH]_o$ and $[HS^-]_o$ are the initial concentrations of CySH and HS^- respectively. Using Eq. (6), we have obtained $k_1 = 3.7 \pm 0.4\ M^{-1}\ min^{-1}$, $k_{-1} = 5.5 \pm 0.6\ M^{-1}\ min^{-1}$, $k_2 = 6.1 \pm 0.5\ M^{-1}\ min^{-1}$ and $k_{-2} = 122 \pm 20\ M^{-1}\ min^{-1}$ at 25°C, pH 10.0 and ionic strength (μ) of 0.17 M.

The temperature dependence of the reaction between CySSCy and HS^- was studied. If the rate constant is expressed as $k_1 = A \exp(-Ea/RT)$, then least-square fit of the data yielded $A = [4.7 \pm 0.3] \times 10^{11}\ M^{-1}min^{-1}$ and $E_a = 15.8 \pm 0.9$ kcal mol^{-1}. The effect of ionic strength on k_1 at pH 10.0 was examined using Bronsted's equation, and the limiting rate constant at zero ionic strength was determined to be $0.38 \pm 0.01\ M^{-1}min^{-1}$. Finally, the effect of pH on k_1 has been studied over a pH range of 7.8 to 12.0. It appears that k_1 does not have a simple $[H^+]$ dependence but is determined by the charge types of both cystine and sulfide at a given pH. Our result suggests that the rate constants for the charged reactant pairs are in the order:

$$CySSCy^{2-}/S^{2-} \sim CySSCy^-/HS^- > CySSCy^{2-}/HS^-.$$

PLANNED ACTIVITIES FOR FY 1987

The above method for the conversion of cystine to cysteine will be further refined when the kinetics and thermodynamics of the steps involved [Eqs. (1)-(5)] become more fully understood. Also, this pro-

cess will be tested for the reduction of other disulfides obtained in the other flue gas desulfurization and denitrification systems.[3]

REFERENCES

1. Tu, M.D., and Chang, S. G. (1987), "Chemistry of a Flue Gas Combined NO_x and SO_2 Scrubber Employing Ferrous Cysteine Additives," *AIChE Environ. Progr.*, 6, 51.
2. Liu, D.K., Frick, L.P., and Chang, S.G. (1987), "A Ferrous Cysteine Based Recyclable Process for the Combined Removal of NO_x and SO_2 from Flue Gas," submitted to *Environ. Sci. Technol.*
3. Chang, S.G., Liu, D.K., Griffiths, E.A., and Littlejohn, D. (1986), "A Process for the Combined Removal of SO_2 and NO_x from Flue Gas," U.S. patent pending.
4. Liu, D.K., and Chang, S.G. (1987), "Kinetic Study of the Reaction Between Cystine and Sulfide in Alkaline Solutions," *Can. J. Chem.*, in press.

The Reaction of Oxygen with Bisulfite Ion in Aqueous Solution*

D. Littlejohn, K.Y. Hu, and S.G. Chang

SO_2 is an unwanted byproduct of the combustion of coal for power generation. To remove the SO_2 from the flue gas before it is released to the atmosphere, it is often scrubbed out by aqueous solutions. An understanding of the oxidation of the dissolved SO_2, in the form of HSO_3^- and SO_3^{2-}, is needed to properly treat the scrubbing liquor.[1]

ACCOMPLISHMENTS DURING FY 1986

The reaction of HSO_3^- with dissolved O_2 was studied using a high-pressure flow system in conjunction with a Raman spectrometer. Use of a high pressure system permitted use of oxygen concentrations sufficiently high to be observed by Raman scattering. The reaction was studied by mixing the HSO_3^- solution with the O_2 solution and passing it through the Raman cell. The solution was either scanned while it was flowing, or the signal of one compound was monitored while the flow was stopped. Spectra of the flowing solution (lower trace) and the stopped solution (upper trace) are shown in Figure 1. ClO_4^- is used as a reference to determine the concentrations of the other ions. The reacted solution shows

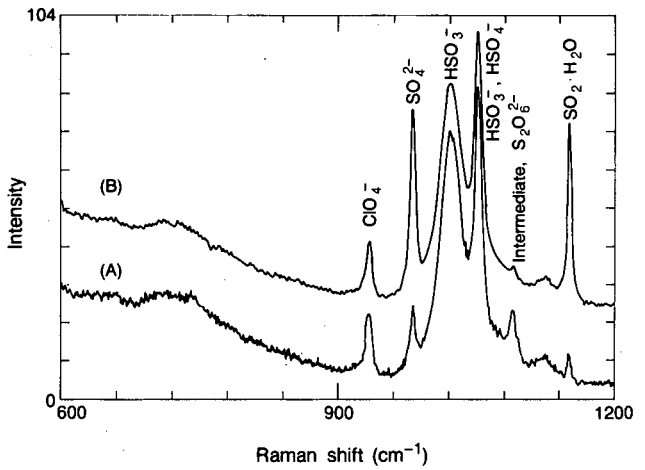

Figure 1. Raman spectra of flowing (lower) and static (upper) reaction mixtures. (XBL 873-9594)

an increase in SO_4^{2-} and SO_2H_2O (from $HSO_3^- + H^+ \rightarrow SO_2H_2O$). It also shows a decrease in the peak at 1090 cm^{-1}, which we found to be caused by an intermediate in the reaction. The intermediate may have the formula of $S_2O_7^{2-}$ and hydrolyze to form sulfate and hydrogen ions

$$S_2O_7^{2-} + H_2O \rightarrow 2H^+ + 2SO_4^{2-}.$$

We have found the intermediate undergoes first order decomposition with a rate constant of $k = .0133 \pm .0026\ sec^{-1}$ at 25°C. The rate of formation appears to have second order dependence on HSO_3^- concentration. The reaction of SO_3^{2-} with O_2 does not form the intermediate and proceeds much more quickly than the reaction of HSO_3^- with O_2.

*This work was supported by the Assistant Secretary for Fossil Energy, Office of Coal Utilization Systems, U.S. Department of Energy under Contract No. DE-AC03-76SF00098 through the Pittsburgh Energy Technology Center, Pittsburgh, PA.

PLANNED ACTIVITIES FOR FY 1987

While the decomposition of the intermediate is fairly well understood, the formation chemistry is still unclear. We plan to do more work on the formation kinetics, including the influence of transition metal ions on the rate.

REFERENCES

1. Huss, A., Lim, P.K., and Eckert, C.A. (1982), "Oxidation of Aqueous Sulfur Dioxide," *J. Phys. Chem. 86*, 4224.

The Acid Hydrolysis and Acid Dissociation Constant of Hydroxysulfamic Acid*

D. Littlejohn, A.R. Wizansky, and S.G. Chang

Bisulfite ions react with nitrous acid in aqueous solution to produce several nitrogen-sulfur compounds.[1] The chemistry of these compounds is important in studies of wet flue gas scrubbing systems and in studies of aqueous aerosols in the troposphere. The reactions involving these compounds are fairly well understood. An exception to this is the acid hydrolysis of hydroxysulfamic acid (HSA). A study of the acid hydrolysis of HSA was made by Candlin and Wilkins.[2] However, some of their experimental runs were done at sufficiently acidic conditions that the protonated form of HSA may have been present.

ACCOMPLISHMENTS DURING FY 1986

We studied solutions of HSA with varying concentrations of $HClO_4$ by laser Raman spectroscopy in an attempt to determine the acid dissociation constant. At pH 1-3, only the 1056 cm^{-1} peak of HSA with a single charge was observed. At more acidic conditions a peak at 1063 cm^{-1} appeared, and the 1056 cm^{-1} peak decreased in magnitude. We attribute the 1063 cm^{-1} peak to fully protonated HSA. The Raman scattering efficiencies of the two forms of HSA were quite similar. From the results obtained, we find a value for the acid dissociation constant for HSA of $K_a = 1.5 \pm 0.5M$.

We also studied the acid hydrolysis of HSA over a temperature range of 25°C to 85°C, using ion chromatography to make determinations of HSA and sulfate ion, one of the hydrolysis products. The hydrolysis reaction was found to have first-order dependence on both HSA and hydrogen ion concentration, and the rate of hydrolysis can be expressed as:

$$-\frac{d[HSA]}{dt} = k[H^+][HSA]$$

where the rate constant, k, can be expressed as $k = A \exp(-E_a/RT)$. A is the pre-exponential factor, E_a is the activation energy, R is the gas constant and T is the temperature. Measurements done at 0.1M and 1.0M acid concentrations yielded differing values of A and E_a, as might be expected with the change in concentrations of the two forms of HSA. The values obtained are listed below.

$[H^+]$	A	E_a
0.1M	5.2×10^{11} $M^{-1}min^{-1}$	21.3 kcal mol^{-1}
1.0M	3.7×10^{14} $M^{-1}min^{-1}$	26.3 kcal mol^{-1}

They are similar to those obtained by Candlin and Wilkins.

The ionic strength dependence of the reaction was studied and found to be less than what would be expected for a reaction between a molecule with a −1 charge and a hydrogen ion. This disparity can also be attributed to the presence of uncharged HSA in solution.

PLANNED ACTIVITIES FOR FY 1987

The study of the reaction has been completed and no further work is planned. The results will be submitted for publication.

*This work was supported by the Assistant Secretary for Fossil Energy, Office of Coal Utilization Systems, U.S. Department of Energy under Contract No. DE-AC03-76SF00098 through the Pittsburgh Energy Technology Center, Pittsburgh, PA.

REFERENCES

1. Chang, S.G., Littlejohn, D. and Lin, N.H. (1982), "Kinetics of Reactions in a Wet Flue Gas Simultaneous Desulfurization and Denitrification System," *ACS Symp. Ser. No. 188*, Washington, D.C., p. 189.
2. Candlin, J.P. and Wilkes, R.G. (1965), "Sulfur-Nitrogen Compounds III. The Acid Hydrolysis of Hydroxylamine N,N-Disulfonate and Hydroxylamine N- and O-Monosulfonates," *Jour.Amer.Chem.Soc. 87*, p. 1490.

The Photoinduced Reaction of H_2S with CO_2 in the Presence of CdS*

D. Littlejohn and S.G. Chang

There has been growing interest in the use of dispersed semiconductors in aqueous solutions to catalyze various reactions, using light as a driving force. Some of these reactions include conversion of CO and CO_2 to CH_3OH and CH_4, and splitting of H_2O. The semiconductor material can absorb light and then undergo charge transfer with the surrounding solution across the solid-liquid junction. The efficiency of the process will be influenced by the overlap of the semiconductor bandgap and the light source and by the energies of the band edges in relation to the redox couples involved in the reaction.

ACCOMPLISHMENTS DURING FY 1986

We have studied the photoinduced reduction of CO_2 to CH_4 in an aqueous CdS dispersion, with H_2S added as a hydrogen source. Other groups have studied the photoreduction of CO_2 in water-based systems but have obtained very low conversion to CH_4. However, sulfur in H_2S is much easier to oxidize than the oxygen in water. An aqueous dispersion of CdS was prepared in an evacuable cell. Reactants were added after the solution was degassed, and the cell was illuminated with the 514 nm line from an Ar^+ laser. After illumination, samples of gas over the solution were analyzed by gas chromatography. The reactions were run in mildly acidic conditions. The results are tabulated below:

Reactant	H_2 quantum yield	CH_4 quantum yield
H_2S	0.4%	
CO_2		<0.009%
$H_2S + CO_2$	0.1%	0.3%

Here, the quantum yield is defined as the number of molecules produced divided by the number of photons absorbed by the solution. The actual quantum yields should be substantially higher, since several photons are needed to convert one CO_2 molecule to one CH_4 molecule.

PLANNED ACTIVITIES FOR FY 1987

Future work will involve studying the influence of pH, temperature and wavelength of light used on the conversion efficiency. The band gap and band edge energies are expected to significantly influence the conversion efficiency. In CdS, these can be changed by doping it with various materials. Also, different semiconductors can be used in place of CdS.

REFERENCES

1. Nozik, A.J. (1978), "Photoelectrocatalytic Reduction of Carbon Dioxide in Aqueous Suspensions of Semiconductor Powders," *Ann. Rev. Phys. Chem. 29*, p. 189.
2. Inoue, T., Fujishima, A., Konishi, S. and Honda, K. (1979), "Photoelectrochemistry: Applications to Solar Energy Conversion," *Nature 277*, p. 637.

*This work was supported by the Assistant Secretary for Fossil Energy, Office of Coal Utilization Systems, U.S. Department of Energy under Contract No. DE-AC03-76SF00098 through the Pittsburgh Energy Technology Center, Pittsburgh, PA.

Controlled Combustion*

N.J. Brown, J.A. Cavolowsky, K. Hom, D. Lucas, A.K. Oppenheim, D.A. Rotman, R.F Sawyer and H.E. Stewart

Principal direction for this program of research is provided by its eventual goal: achievement of a significant technological advancement by the development of controlled combustion systems. It is worth noting that any progress made in this respect should be of definite benefit to combustion technology.

The principle is quite straightforward. The current state-of-the-art in combustion technology is manifested by combustors utilizing fully established flames–the form under which combustion is best known to occur in nature. But the salient feature of this process is the evolution of exothermic energy and its deposition in the working substance; whereas flames accomplish this by concentrating the active chemical reaction, as measured for example by the effective width of the pulse in the concentration of active radicals or exothermic power, within a very narrow zone. The essential purpose of our studies is to develop means whereby the zone of chemical activity would be spread out, so that its distribution in space and time could be kept under proper control. Combustors of this kind would not act merely as sources of power–as they do universally today–but they would also provide service as fully controllable chemical reactors.

Practically, this can be achieved by means of either multipoint ignition, product recirculation, or the use of additives, as well as any of their combinations. Although they are, of course, principally chemical in nature, their success depends crucially on the control of the fluid mechanical conditions under which they are administered. For this reason, major emphasis in our studies is placed upon what we like to refer to as the *Aerothermodynamics of Combustion.*

Our previous studies in this field elucidated the salient features of ignition and revealed the essential mechanism of the formation and propagation of flames under turbulent flow conditions, as is typical of all the technologically viable combustion systems. Of particular interest here is the effect of stretch–the pulling apart of the flame front by the flow field in which it resides. Dynamically, flames act as sources of velocity and vorticity. It is primarily as a consequence of the latter that their fronts become established as connected surfaces on the contours of large-scale vortex structures that form the most prominent feature of turbulent combustion fields.

As to the actual feedback control devices, one of the best candidates is plasma jet igniters, for they require the minimum amount of time (few tens of microseconds) to become fully active. Principal accomplishments we achieved last year include progress in experimental studies of such igniters, as well as in numerical analysis of combustion fields in internal combustion (IC) engines.

ACCOMPLISHMENTS DURING FY 1986

Plasma Jets

Formation of pulsed plasma jets, or puffs, was examined using several visualization techniques.[10] Self-light streak photography was first employed to record salient global features of the development and structure of the jet. This provided information on the motion of the luminous gas particles in its core, revealing that plasma jets can have two distinct modes, being either totally subsonic or embodying a supersonic efflux manifested by the recorded streaks of Mach discs. At a fixed power pulse of electrical energy discharge in the plenum chamber, the outcome depended on the constriction imposed by an orifice at its outlet. Whereas the difference between the two types of jets was quite small, penetration in the subsonic case was found to be definitely larger than in supersonic. The turbulent evolution of the puffs was thereupon explored by ultra-high frequency (200 kHz) schlieren cinematography, using our unique system employing a pulsating ruby laser as the light source and a rotating mirror camera as the recorder.

In order to reveal the full history of the generation of a plasma puff from the electric discharge in the cavity to the formation of the jet at its outlet, a transparent cavity generator made out of quartz plates was built of rectangular cross section, 2 mm x

*This work was supported by the Office of Energy Research, Office of Basic Energy Sciences, Engineering and Geosciences Division of the U.S. Department of Energy under Contract No. DE-AC03-76SF00098, and by the National Science Foundation under Grant CPE-8115163.

2 mm. A cinematographic record of the process under study, obtained by the use of this device is shown in Fig. 1. The electric arc, appearing initially in the first frame, is unstable as it sways to and fro from one side of the grounding plate to the other. Close examination of frame 2 shows a cylindrical shock emanating from the arc heating the gas in the cavity. Further heating of the gas by the arc forms diffusion waves that stretch across the width of the cavity. As depicted in frame 3, in about 10 μsec the temperature and the pressure in the cavity rise sufficiently to expel the gas, forming a jet.

Flame Propagation

In the piston-compressed charge contained in the cylinder of an IC engine, the flame cannot be considered as truly laminar. Its most prominent feature is that it is stretched, i.e., it becomes distorted by the flow field in which it resides.[8] The latter is, in turn, due primarily to the action of the flame itself. So the sequence of events is closed. First the flame is formed; then it generates the flow field that subsequently pulls its front apart–an effect that can eventually produce its extinction by overstretching.

All that is best illustrated by the results of numerical modelling of the process as it occurs in a variable volume enclosure of an IC engine, Fig. 2, depicting the process of flame propagation, associated with the evolution of the flow field portrayed by an array of velocity vectors. The pressure pulse evaluated concomitantly turned out to be in remarkably good agreement with the transducer record obtained in an engine operating under conditions for which the numerical analysis was performed.

PLANNED ACTIVITIES FOR FY 1987

In furthering our program of research pertaining to controlled combustion processes, we plan to conduct three phases of work.

1. Measure hydrogen atom concentration profiles in plasma puffs injected into an inert atmosphere, as well as into a combustible mixture, by the use of the molecular beam mass spectrometer.
2. Investigate the formation of a spray of fuel and its ignition at high pressures and elevated temperatures by the use of the shock tube apparatus described in last year's Annual Report.
3. Study the aero-thermo-chemico-dynamic processes of combustion by numerical modeling analysis.

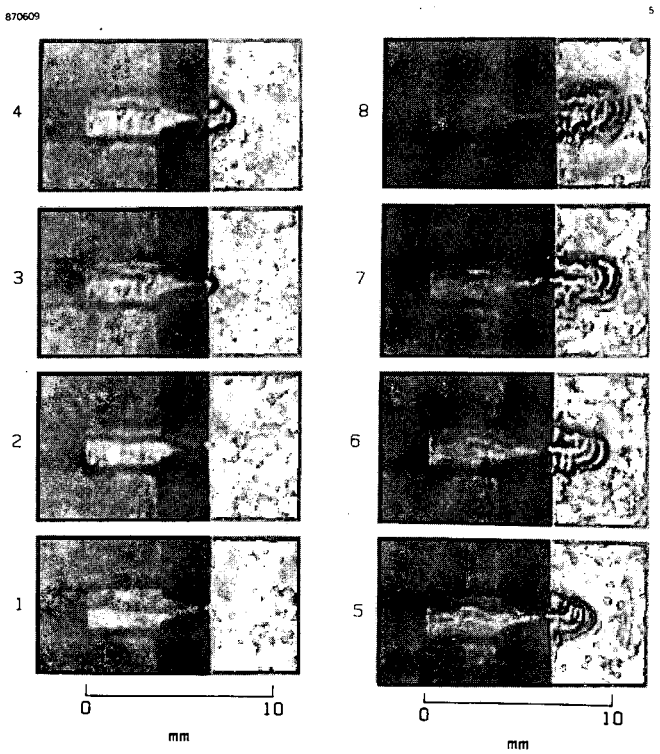

Figure 1. Cinematographic schlieren records of plasma discharge in the plenum chamber of a jet igniter and the ensuing jet plume. (Time interval between frames: 5 μsec) (XBB 873-2182)

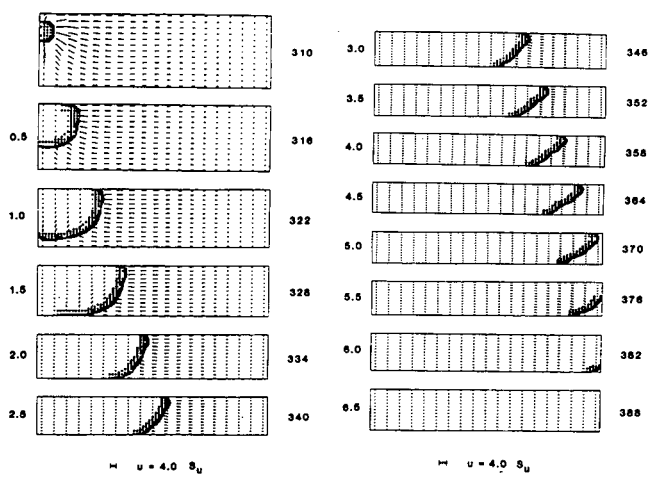

Figure 2. Sequence of numerical solutions depicting the process of flame propagation and the concomitant evolution of the flow field, as displayed by the array of velocity vectors, in the cylinder of an internal combustion engine. (XBL 873-1220)

REFERENCES

1. Forsha, M.D., Sawyer, R.F., and Oppenheim, A.K. (1986), "Fuel Injection System for Shock Tube Studies of the Ignition of Preheated Fuels," Applied Science Division, LBL-21103.
2. Parker, T.E., Sawyer, R.F., and Oppenheim, A.K. (1986), "Thermodynamic Properties of Hydrocarbons," Applied Science Division, LBL-21104.
3. Lucas, D., Cavalowsky, J.A., Edwards, C.F., and Oppenheim, A.K. (1986), "Species and Temperature Measurements in a Pulsed Plasma Jet by Molecular Beam Mass Spectrometry," *Combust. Sci. and Tech., 50,*, p. 27.
4. Oppenheim, A.K. (1986), "The Beauty of Combustion Fields and Their Thermodynamic Significance," *Dynamics of Reactive Systems Part I: Flames and Configurations* (J.R. Bowen, J-C. Leyer, and R.I. Soloukhin, Editors) Progress in Astronautics and Aeronautics, *105,* AIAA, New York, p. 3.
5. Creighton, J.R. and Oppenheim, A.K. (1986), "On the Role of the Radical Pool in Combustion," *Dynamics of Reactive Systems Part I: Flames and Configurations* (J.R. Bowen, J-C. Leyer, and R.I. Soloukhin, Editors) Progress in Astronautics and Aeronautics, *105,* AIAA, New York, p. 304.
6. Cavolowsky, J.A., Breber, P.R., Oppenheim, A.K., and Lucas, D. (1986) "Pulsed Plasma Jet Igniters: Species Measurements in Nitrogen and Air," Applied Science Division, LBL-21899.
7. Lee, H.-S., Fernandez-Pello, A.C., and Oppenheim, A.K. (1986) "Stagnation Point Evaporation of a Liquid Fuel at Near and Super-Critical Conditions," ASME Paper No. 86-WA/HT-15, New York.
8. Oppenheim, A.K. and Rotman, D.A. (1987) "Aerothermodynamic Properties of Stretched Flames in Enclosures," XXIst Symposium (International) on Combustion, The Combustion Institute, Pittsburgh, Pa., in press.
9. Oppenheim, A.K. and Rotman, D.A. (1987) "Fundamental Features of Ignition and Flame Propagation in Engines," ASME Paper No. 87-ICE-21, New York.
10. Cavalowsky, J.A., Faris, D., Smy, P.R., and Oppenheim, A.K. (1987) "Formation of a Plasma Puff," SAE Paper 870609.
11. Oppenheim, A.K. (1987) "Fluid Mechanical Control of Combustion," Plenary Lecture, 11th Canadian Congress of Applied Mechanics, Edmonton, Canada.

Smoke Emission Factors from Burning Wood and Asphalt as Measured in Medium Scale Experiments*

R.B. Williamson, R. Dod, F.W. Mowrer, N.J. Brown, and T. Novakov

The concept of "Nuclear Winter" has been postulated with a number of assumptions regarding the smoke produced by post- nuclear exchange fires[1,2]. Whether Nuclear Winter will occur in the aftermath of a nuclear exchange depends largely on the quantity of smoke generated, its distribution in the atmosphere and its optical characteristics. The present state of knowledge regarding smoke production from building fires is low. Most of the current information stems from small-scale fire research with no correlating data for larger scales on the order of actual buildings. With rare exception, the existing small-scale data do not include size distribution of smoke particles, information essential for global effects modeling.

A series of medium-scale fire experiments with representative urban fuels, such as wood and asphalt roofing shingles, has been conducted here at Berkeley. The objective of this study has been to measure the quantity of smoke emission by collecting smoke samples as a function of mass loss of the fuel.

ACCOMPLISHMENTS DURING FY 1986

During 1986, a total of 13 experiments were conducted at the Fire Research Laboratory at the Richmond Field Station with plywood, wood cribs and asphalt roofing shingles to determine the amount of smoke that was produced when these fuels burned.

*This work was supported by the Defense Nuclear Agency, through the U.S. Department of Energy under contract No. DE-AC03-76SF0098.

In addition to the smoke measurements the rate-of-heat-release (RHR) was measured using oxygen depletion calorimetry (ODC)[3]. Some of the experiments were well ventilated while others had reduced ventilation that would occur for fires in buildings.

The mass of smoke in each experiment was determined by sampling the aerosol particulate in the exhaust duct which captured all of the effluent from the burning material. Sampling probes were inserted through the wall of the duct and were designed to provide isokinetic sampling of the flowing smoke and combustion products. The smoke particulate was captured on filters and in a cascade impactor, and then weighed so that the quantity of smoke produced by burning a unit mass of fuel, called the "smoke emission" factor, could be given for each fuel.

The carbon content of the samples was characterized by a thermal evolved gas analysis (EGA). This technique has been shown to be able to characterize collected aerosol carbon particles by type: organic, "black", or carbonate carbon[5,6]. All the samples analyzed in this study showed a dominant black carbon peak and no carbonate, allowing for the differentiation of black from organic carbon to be made in an unambiguous manner.

An indication of the reliability of the the sampling procedure can be obtained from a comparison of the total particulate carbon emission factors as determined from the duct total filter (front filter in the stack) and the sum of the carbon collected in the impactor. For fires without ventilation restriction the agreement is good, with the sum of impactor carbon equal to 92 ± 7% of that collected by the total filter. This agreement also implies that the particle concentration in the duct is uniform at the location of the probe inlets.

The smoke emission factors measured for all of the experiments are shown in Fig. 1. The first bar, labelled "WOOD", in Fig. 1 represents the smoke emission for a wood crib burned in the open with adequate ventilation is approximately 0.1% for the total emission with 0.05% for the more important "black" graphitic carbon. The next bar in Fig. 1 is that for plywood burned under adequate ventilation conditions which shows 0.2% total emission factor with half of that being black graphitic carbon. When wood cribs are burned under limited ventilation conditions the emission factor is increased to over 3.5% total and 2.7% black carbon, and this is shown in Fig. 1 by the bar labelled "WOOD*". Finally the total emission factor for asphalt shingles is almost 14% with 10% being black carbon. It is apparent that the asphalt shingles produce almost ten times

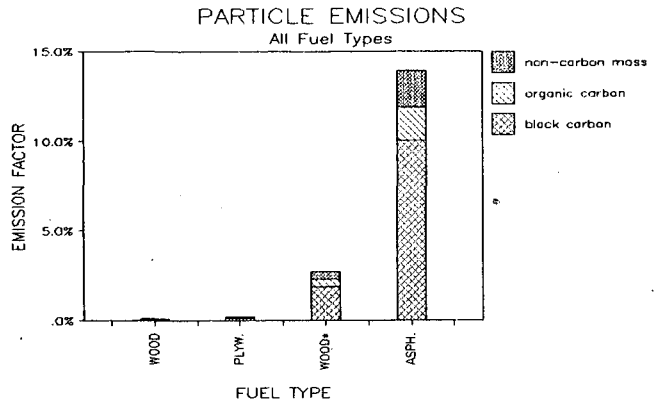

Figure 1. Histogram of the smoke emission factors, (i.e., mass of smoke particulate per unit mass of fuel burned), measured for whole wood cribs, plywood and asphalt roofing shingles. Wood* refers to wood cribs burned under restricted ventilation conditions. (XBL 873-889)

more smoke than the wood cribs burned under limited ventilation conditions, and on the order of one hundred times the smoke produced by wood products under adequate ventilation conditions.

The implications of the measurements presented above, in the context of Nuclear Winter, are centered around three aspects of the measurements. First there is a substantial effect of ventilation on the smoke production from burning wood; smoke emission factors measured under limited ventilation conditions were more than an order of magnitude higher than those measured in well ventilated conditions. Wood is one of the major building and furnishing materials used in the United States, and it is reasonable to assume that large quantities of wood will burn under both limited and unlimited ventilation conditions in the post nuclear environment. A second aspect of the measurements is that the "medium-scale" well ventilated wood experiments produced several orders of magnitude more black carbon than previously reported bench-scale experiments[5]. A third aspect of the measurements is that the smoke emission factors found for asphalt roofing shingles, a total of almost 14% with 90% being black carbon, may have a significant impact on urban smoke production in the post nuclear environment.

The morphology of the smoke particles produced in these experiments have been observed by both optical and electron microscopy, and appear to be similar to other high black carbon soot particles with an open lace-like appearance. A separate report is being prepared on this topic. It is important to note that the morphology of wood smoke from these medium-scale experiments is different than the morphology observed from bench-scale experiments[7].

PLANNED ACTIVITIES FOR FY 1987

This work is scheduled to continue, and in 1987 new urban fuel materials will be evaluated and larger fuel masses of wood and asphalt will be burned under various ventilation condition in order to evaluate the effects of scaling.

REFERENCES

1. Turco, R.P., Toon O.B., Ackerman, T.P., Pollack, J.B. and Sagan, C. (1983), *Science, 222,* p. 1283.
2. Turco, R.P., Toon O.B., Ackerman, T.P., Pollack, J.B. and Sagan, C. (1984), *Scientific American, 251,* p. 33.
3. Parker, W.J. (March 1982), "Calculations of the Heat Release Rate by Oxygen Consumption for Various Applications," NBSIR 81-2427-1.
4. Huffman, E.W.D. (1977), *Michrochemical Journal, 22,* p. 567.
5. Dod, R. L., and Novakov, T. (1982), *Industrial Applications of Surface Analysis,* p. 397.
6. Novakov, T. (1981), *Nature, Aim and Methods of Microchemistry,* p. 141.
7. Williamson, R. B., Rashed, A., Mowrer, F. W., and Novakov, T., "Morphology of Smoke Particles from Bench-Scale Experiments," Paper presented at the poster session of the 21st International Symposium on Combustion, Munich, West Germany, August 3-8, 1986.

Combustion Chemistry*

N.J. Brown, O. Rashed, A.S. Edlin, and D. Lucas

Combustion chemistry consists of complex chain mechanisms involving radical and stable species. The inherent difficulties encountered in performing measurements in high temperature environments where the chemistry is frequently coupled to fluid mechanics makes the study of combustion chemistry in realistic combustion systems difficult. The application of various theoretical approaches to the study of thermal and state-to-state reactions is particularly attractive for elementary reactions and processes important in combustion because it offers the long-term possibility of prediction. This approach is further strengthened when it is coupled with an experimental program to verify the theoretical predictions. The approach of our program has been to pursue research in theoretical, modelling, and experimental areas.

ACCOMPLISHMENTS DURING FY 1986

We have performed complete Monte Carlo quasi-classical dynamics (MCQCD) studies of the $H_2 + OH$ reaction and computed rate coefficients over the temperature range 600-4000 K. In contrast to our previous calculations[1-3], no state-to-state rate coefficients were determined, but rather a Monte Carlo average was performed over the entire phase space including the relative translational velocity and the rotational and vibrational states of the two-molecule system. The rate coefficients computed from the MCQCD calculations were compared with those computed statistically using a hierarchy of approximations[4-6]. The highest level of statistical approximation was microcanonical J-conserving transition state theory with one-dimensional tunneling (MJTT), and in this, the tunneling probability is properly convolved with the number of states to correct for tunneling in a manner that is very similar to a quantum tunneling correction. Tunneling corrections were those associated with parabolic and Eckart barriers. Microcanonical J-conserving (MJT) transition state calculations were performed without tunneling and with a multiplicative Wigner correction. In addition, canonical transition state calculations with (CTW) and without (CT) Wigner tunneling corrections were performed. The statistical calculations were performed with the saddle point characteristics of the ab initio and fitted potential energy surfaces.

Rate coefficients computed via MCQCD gave good agreement with experimental values for $T > 1500$ K. We are still exploring reasons for the disagreement at the lower temperatures. The effects of conserving energy and angular momentum decrease the rate coefficient, in general, CTW > MJTT = CT > MJT as shown in Fig. 1. At $T < 300$ K, the computed MJTT rate coefficient (ab initio surface parameters) is larger than the experimen-

*This work was supported by the Director, Office of Energy Research, Office of Basic Energy Sciences, Chemical Sciences Division of the U.S. Department of Energy under Contract No. DE-AC03-76SF00098.

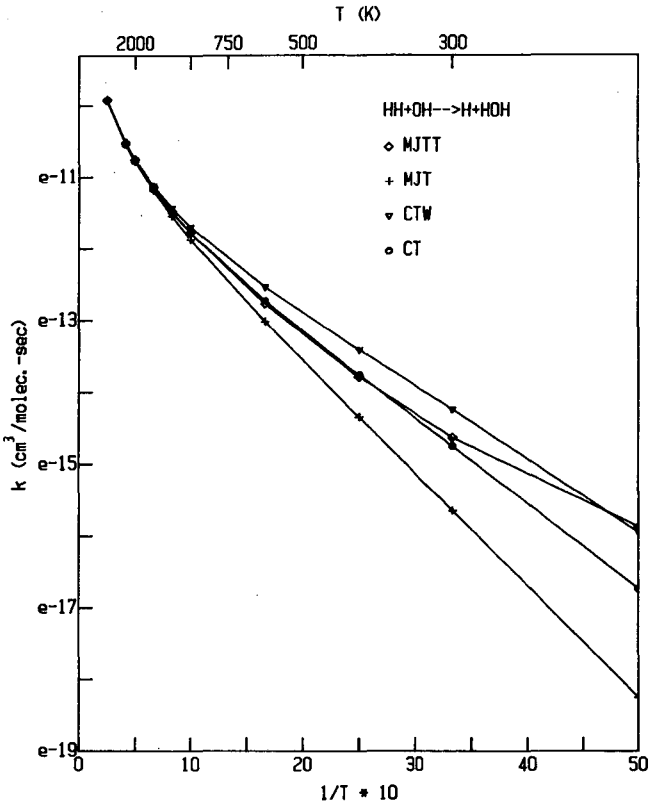

Figure 1. Arrhenius plot of the $H_2 + OH \rightarrow H_2O + H$ rate coefficient ($10cm^3$/mdec·sec) for various levels of statistical approximations. (XBL 873-1221)

tal value, but gives satisfactory agreement with experimental values for temperatures up to 2000 K. At larger temperatures, computed rate coefficients are larger than experimental values due to recrossing effects. The MJTT rate coefficients computed with the parameters of the fitted surface are smaller than experimental values for T < 750 K and agree quite satisfactorily with experimental values for T < 4000 K. Comparison of the ab initio and fitted results reveals the significance of small differences in the transition state geometry and frequencies. Tunneling corrections persist for temperatures as high as 1500 K. For T < 1000 K, the order of the tunneling corrections is parabolic barrier > Eckart barrier > Wigner correction. Although direct comparison is complicated by using different theoretical approximations, the results of different approaches are in agreement over the range of temperatures important for combustion.

The same techniques were used to investigate isotope effects for the reactions: HD + OH, D_2 + OH, H_2 + OD, HD + OD[7]. Agreement between the MCQCD calculations and experimental rate coefficients is poor for H_2 + OH and D_2 + OH at T < 1200 K, but agreement between MCQCD calculations and experimental values of isotopic ratios is satisfactory at low temperatures. The order of rate coefficients computed with different levels of statistical theory is: CTW > MJTT > CT > MJT, at 200 K, CTW and MJTT often change places. At T > 1000 K, the four methods yield nearly identical rate coefficients. The isotope effects are explained by tunneling, intramolecular, and intermolecular effects. At low temperatures, tunneling can exert an important effect upon isotope ratios. Since the magnitude of the imaginary frequency of HDOH, DDOH, and HDOD is on the order of 1100 cm^{-1} and is 1500 cm^{-1} for HHOH, the isotopic ratios for these species are large at low temperatures where tunneling corrections are important. Agreement between calculated MJTT and Ravishankara et al.[8] experimental rate coefficients is satisfactory for H_2+OH and D_2+OH. Inverse isotope effects are found for DH + OD → (DHOD) → D + HOD and HH + OD → (HHOD) → H + HOD for T < 1000 K. The magnitude of the imaginary frequency for these transition states is nearly equal to that of HHOH. The two-channel reaction HD + OD yields an inverse isotope effect over the entire temperature range, and the ratio approaches .87 at high temperatures. Examining the individual channels reveals that the rate coefficient for the production of HOD is greater than that for DOD with the former exhibiting an inverse isotope effect for T < 600 K. The branching ratio k_{HOD}/k_T decreases with temperature, approaches a nearly constant value of 70 %, and is slightly increased by tunneling. The two channel reaction HD + OH exhibits a very small isotope effect. The HOH channel rate coefficient is greater than the DOH channel, and the branching ratio k_{HOH}/k_T decreases with temperature and approaches a nearly constant value of 60 % and is increased by tunneling.

The ignition of ozone/hydrogen/oxygen mixtures in a constant volume cell was investigated[9]. Ozone, the only significant absorber in this system, is photolyzed and produces oxygen atoms which initiate combustion. Light was focussed into heated and unheated aluminum cells with optical windows by MgF_2 or UV grade lenses of various focal lengths. Mixtures having total pressures in the range 25 to 250 torr were investigated. The mole fraction of ozone needed to initiate reaction was found to be essentially constant over the entire pressure range investigated. These results, and others comparing ignition properties of various fuels, confirm that the laser ignition process is fundamentally different from thermal and spark ignition cases.

Preliminary experiments were conducted in an attempt to use other gases as absorbing species. Mixtures with species such as hydrogen iodine and methane ignited, but photolysis was determined to be a multiphoton event rather than the desired and readily controllable single photon absorption. The most promising candidate for future experiments is nearly pure hydrogen peroxide.

PLANNED ACTIVITIES FOR FY 1987

A new study using functional sensitivity analysis to determine the relationship between structure in a potential energy surface and classical mechanical observables has been undertaken in collaboration with Professor Herschel Rabitz and Richard Judson of Princeton University. Studies of a two molecule system capable of undergoing a variety of energy transfer processes and reactions are being pursued. The $H_2 + H_2$ (H4) system has been selected for study because there are four semi-empirical valence bond surfaces for this system determined by Silver and Brown[10], there is renewed interest in experimentally investigating energy transfer in this system, and a new ab initio potential energy surface will be computed for this system by investigators at SNL. The studies will proceed in a hierarchical fashion: (1) a 2D rigid rotator, (2) a vibrating rotator, and (3) 3D energy transfer studies. Reactivity will be investigated by examining energy deposition in the product species, and will most likely be studied in two and three dimensions.

REFERENCES

1. Rashed, O. and Brown, N.J., (1985), "A Molecular Dynamics Study of the Reaction $H_2 + OH \rightarrow H_2O + H$," *J. Chem. Phys., 82,* p. 5506.
2. Brown, N.J. and Rashed, O., (1986), "Intra- and intermolecular Energy Transfer in $H_2 + OH$ collisions," *J. Chem. Phys., 85,* p. 4348.
3. Rashed, O., (1986), "Reactivity and Energy Transfer in the $H_2 + OH$ System," Ph.D Thesis, Department of Mechanical Engineering, University of California, Berkeley.
4. Miller, J.A., Parrish, C., and Brown, N.J, (1986), "A Statistical-Theoretical Rate Coefficient and Branching Ratio for the Reaction $O + HCN \rightarrow$ Products," *J. Phys. Chem., 90,* p. 3339.
5. Miller, J.A., Melius, C.F., and Brown, N.J., (1986), "A Theoretical Prediction of Rate Coefficients for Reactions Involving Intermediate Complex Formation," *Abstracts, 9th International Symposium on Gas Kinetics, Abstract A5.*
6. Brown, N.J., Rashed, O., and Edlin, A., (1986), "Quasi-classical and Transition State Calculations of the $H_2 + OH \rightarrow H_2O + H$ Rate Coefficient." *PS105 Twenty-first Symposium (International) on Combustion, Munich, Germany.*
7. Brown, N.J., Rashed, O., and Edlin, A., (1986), "A Theoretical Study of Deuterium Isotope Effects in the Reaction $H_2 + OH \rightarrow H_2O + H$," *Second Workshop on Modelling of Chemical Reaction Systems, Abstracts. Heidelberg, Germany*
8. Ravishankara, A.R., Nicovich, J.M., Thompson, R.L., and Tully, F.P., (1981), "Kinetic Study of the Reaction of OH with H_2 and D_2 from 250 to 1050 K," *J. Phys. Chem., 85,* p. 2498.
9. Lucas, D., Dunn-Rankin, D., Hom, K., and Brown, N.J., (1986), "Ignition by Excimer Laser Photolysis of Ozone," *Accepted for publication in Combustion and Flame. Also PS153, Twenty-first Symposium (International) on Combustion, Munich, Germany. Also WSS-86-36, Fall Meeting of the Western States Section/Combustion Institute, Tucson, Arizona. Also LBL 20871.*
10. Silver, D.M., and Brown, N.J., (1980), "Valence Bond Model Potential Energy Surface for H_4," *J. Chem. Phys., 72,* p. 3859.

Combustion Fluid Mechanics*

R.K. Cheng, P. Cho,‡ I. Gokalp,†† J.R. Hertzberg, C.K. Law,‡ M.Z. Pindera, I.G. Shepherd,† F. Robben, and L. Talbot

Although it is well known that fluid mechanical turbulence increases the overall combustion reaction rate, the exact relationship between turbulence intensity and mean heat release rate remains an unresolved issues in fundamental turbulent combustion research. The overall goal of this program is to gain a better physical understanding of the interaction between turbulence and combustion through detailed study of the complex turbulent combustion flowfields in simplified laboratory scale burners using laser diagnostic techniques. The results are also used to compare with the predictions of theoretical models.

ACCOMPLISHMENTS DURING FY 1986

The experiments conducted in FY 1986 are focused on measuring the characteristics of the temporal fluctuations. These studies are motivated by recent development in numerical models which have proposed the use of the flame passage time frequency, ν, to model the heat release rate. Experimental data are needed to validate the modeling assumption and to assist in formulating the relationship of ν with mixture and turbulence parameters. In our experiments, two diagnostic techniques were used to measure the passage time frequencies in turbulent v-flames[1] and in stagnation flow stabilized flames.[2] Also obtained were the frequency spectra of the velocity and scalar fluctuations to study the effects intermittent flame passage on the velocity spectra.

The first diagnostic method used for studying flame movements is the Linear Array Rayleigh Scattering (LARS)[3] technique which measures instantaneous density profiles across the turbulent flame at rates of up to 5 kHz. It was used to determine the instantaneous flame front position directly and makes possible the time resolved study of flame front oscillation frequencies. Methane/air premixed turbulent v-shaped flames at an approach velocity of 2 m/s and a range of inlet turbulence levels and equivalence ratios, ϕ from 5%-8% and 0.6-0.8, respectively, were studied.

The statistics of the flame front position were obtained by extracting the flame boundary from the images and generating a probability density function of its distance from the mean. A comparison of the spectra of the flame front oscillations and the cold flow velocity is shown in Fig. 1. The results indicate that the inlet turbulence controls flame motion at frequencies between 100 and 1000 Hz. Changes in heat release for a given inlet turbulence increase the amplitude of the flame fluctuations without modifying the spectral characteristics.

For premixed turbulent v-flames with higher approach velocities of up to 5.5 m/s, the flame passage time frequencies were measured using a point measurement method based on Mie scattering from silicone oil droplets which evaporates and burns through the flame front[1]. Also deduced are the intermittency which is the probability of encountering the burned state, the probability density distributions of the time periods spent in the burned and the unburned states and the passage time frequency, ν, which is the number of flame transitions observed in a given time period. All of these data are needed for further development of the numerical model of Bray, Libby and Moss.[4]

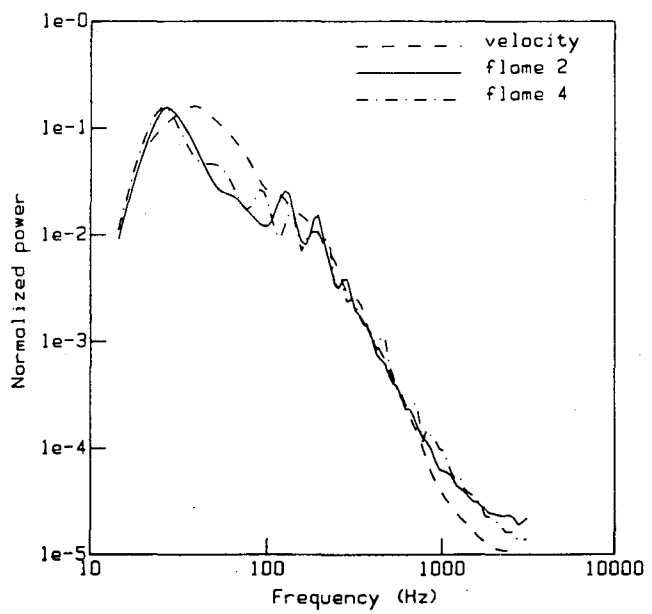

Figure 1. Spectra of flame oscillation from two methane/air turbulent v-flames, flame 2 with equivalence ratio, $\phi = 0.6$ and flame 4 with $\phi = 0.7$, both propagating in perforated plate turbulence of 8% intensity. (XBL 871-315)

*This work was supported by the Director, Office of Energy Research, Office of Basic Energy Sciences, Chemical Sciences Division of the U.S. Department of Energy under Contract No. DE-AC03-76SF00098. ‡ Department of Mechanical Engineering, University of California, Davis. †† CRCCHT-CNRS Orleans, France † Department of Mechanical Engineering, University of California, Berkeley.

For a near stoichiometric (ϕ=0.98) methane/air v-flame with 5 m/s approach flow velocity and turbulence intensity of 8%, typical flame passage frequencies at the center of the flame brush average about 700 Hz. Near the flame stabilizer, ν is about 800 Hz. With increasing distance from the stabilizer, ν decease almost linearly to 600 Hz at positions further downstream. The distribution of ν across the flame brush is found to follow closely the function used in the numerical model $\nu(c) = c(1-c)$ where c is the progress variable which is identical to the intermittency for premixed turbulent flames. However, the experimental distributions of ν is not symmetrical about $c = 0.5$ but skewed towards the burned ($c > 0.5$) region. This skewness may be associated with the shapes of the flame cusps which point towards the burned state.

The flame passage time frequencies were also measured in the stagnation point stabilized premixed turbulent flames. Under similar conditions as those mentioned above for the v-flame study, typical value of ν at the flame brush center was 130 Hz, almost an order of magnitude lower. The reason for the drastic differences in ν for the two configurations can be explained by the fact that in the v-flames, the flame wrinkles are convected along the flame brush at velocities close to that of the approach flow. In the stagnation flame the tangential velocity at the centerline of the burner where the data were taken is zero. The movements of the flame wrinkles are caused only by oscillations of the turbulent eddies about the centerline. Hence, even if the flame wrinkle sizes were comparable in the two configurations, the passage time in the v-flame would be much shorter due to the convection velocity.

The Mie scattering signals were also analyzed by fast Fourier transform to obtained the intermittency spectra in the v-flame. Shown in Fig. 2 is a comparison of the energy spectrum of the velocity component normal to the flame brush with the corresponding intermittency spectrum for a stagnation flow stabilized methane/air flame (ϕ=0.98) propagating in perforated plate turbulence (U_{rms}=8%). Both spectra peak at about a wave number, k, of 100. The inverse of the most energetic wave number $l_e = 1/k_e$ represents the mean size of the energy containing eddies. In this case l_e = 1.0 cm which is similar to the turbulent flame brush thickness but larger than the 3.0 mm integral scale of the incident turbulence.

In addition to the temporal fluctuation measurements, intermittency and conditioned velocity statistics were also obtained for four methane/air flames in the stagnation flow configuration. The stagnation

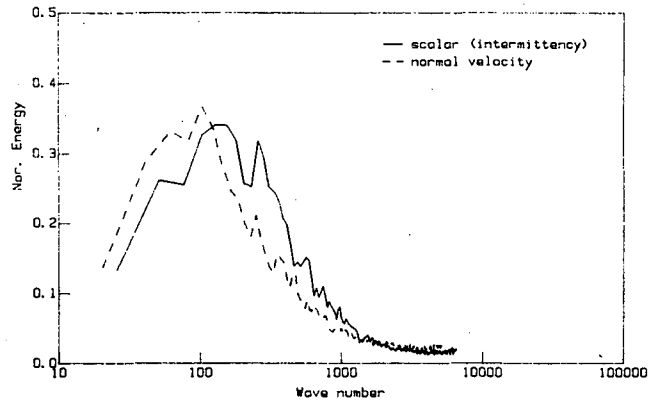

Figure 2. Comparison of the intermittency and velocity spectra in a methane/air flame (ϕ = 0.98) stabilized in a turbulent (intensity of 8%) stagnation flow. (XBL 871-316)

plate for all cases was placed at 75 mm from the exit of the flow nozzle. The approach flow velocity at the exit was 5.0 m/s and turbulence was generated by a grid or perforated plate. Two mixtures, a near stoichiometric flame ϕ=0.98 and a lean mixture ϕ=0.75 were used. The intermittency, which was measured by the Mie scattering technique above mentioned, was used to infer the flame brush thickness. The data also provided a precise definition of the flame brush boundary for determining the turbulent burning speed. The results showed that the flame boundary coincides with the point at which the axial velocity profiles reach a local minimum. This demonstrated that the criterion used for defining the laminar flame speed is also valid for defining the turbulent burning speed.

The conditional velocity statistics were measured using the LDA technique described in Ref. 1. The overall features of the conditional velocity statistics in the stagnation flow stabilized flames are similar to those observed in the v-flame and Bunsen flame. The increase in rms fluctuations within the flame zone is observed only for the axial component which is normal to the flame brush. The tangential rms fluctuation remains relatively constant through the flame but increases rapid towards the wall. The unconditioned velocity joint probability density function (jpdf) for the rich flames are distinctly bimodal. The bimodality of the jpdfs for the leaner flames is less distinct.

In addition to our experimental works, a numerical study of the effects of vorticity in premixed flame using the vortex dynamic technique has also been completed. In this analysis, the diffusion of heat and species is ignored and so the behavior of the flame and the surrounding gases can be described using

only the conservation of mass and momentum equations, and by specifying the appropriate flame speed. Applying the general velocity decomposition principle, which treats the flowfield as comprising of distinct volumetric, rotation, and potential components, a model was developed in which the flame was treated as a surface source of volume. The effects of vorticity production on the velocity field were illustrated in numerical simulations of a laminar stagnation flame and a v-shaped flame with and without turbulence in the approach flow. The results indicate that for the flames of finite extent, the production of vorticity forms an integral part of the overall velocity field. Ignoring the effects of fluid rotation can lead to results not in accord with the experimental results obtained from the v-flame.

PLANNED ACTIVITIES FOR FY 1987

Experimental studies of temporal fluctuations in the v-flame and in the stagnation flow stabilized flame will be continued. The flame configurations will also include the large Bunsen flames, in addition to the v-flame and stagnation flow stabilized flames to investigate the effects of flame geometry. Although the measurement of the flame passage frequencies and their distributions using a single point technique is expected to provide much insight into the temporal structures of the turbulent flames, the study of spatial structures is also needed to gain a more complete understanding of the flame front dynamics. In FY 1987 we plan to conduct a tomographic study of the flame front dynamics and flame structures using a video camera system interfaced with the image analysis system. As discussed earlier, the shape and size of the flame wrinkles and their convection speed influence the flame passage time frequencies.

The vortex dynamics simulation of the V-flame and the stagnation point stabilized flame will be extended to include the effects of incident turbulence. The treatment of the flame front will be the same as described earlier. In addition to including the vorticity jump across the flame front, the variation of the flame speed by flame stretch (fractional change of the flame surface area with time) will also be included.

The study of non-premixed (diffusion) turbulent flame will be initiated. This study is a logical extension of our program into the other significant mode of turbulent combustion. Our approach is to investigate non-premixed turbulent flames at moderate to low Reynolds numbers. All of the diagnostics techniques and associated data reduction methods can be used for this study. A turbulent jet flame burner with adjustable co-flowing air will be constructed.

REFERENCES

1. Cheng, R. K. (1984), "Conditional Sampling of Turbulence Intensities and Reynolds Stress in Premixed Turbulent Flames," *Combustion Science and Technology, 41,* p. 109.
2. Cho, P., Law, C.K., Hertzberg, J.R. and Cheng, R.K. (1986), "Structure and Propagation of Turbulent Premixed Flames Stabilized in a Stagnation Flow", *21st Symposium (International) on Combustion.*
3 Shepherd, I.G., Hubbard, G.L. and Talbot, L. (1986), "The Dynamic Structure of Turbulent V-shaped Premixed Flames," *21st Symposium (International) on Combustion.*
4. Bray, K.N.C., Libby, P.A. and Moss, J.B. (1984), "Flamelet Crossing Frequencies and Mean Reaction Rates in Premixed Turbulent Combustion," *Combustion Science and Technology, 41,* p. 143.
5 Pindera, M. Z. and Talbot, L. (1986), "Flame Induced Vorticity: Effects of Stretch", *21st Symposium (International) on Combustion.*

Redox Reactions and Bioenergetic Studies on the Photochemical Conversion of Solar Energy*

L. Packer, I. Fry, R. Mehlhorn, J. Maguire, S. Belkin,† R. Giauque, J. D'Souza,‡ W. Nitschmann, E. Hrabeta-Robinson, M. Huflejt, and J. Hrabeta

The Membrane Bioenergetics group is currently investigating several research topics, which range from the determination of the molecular events during proton translocation by bacteriorhodopsin, to the biochemical and physiological response of freshwater cyanobacteria to environmental stress imposed by salinity and toxic elements. Only a brief overview of our most recent and novel results will be given here, along with an extensive reference list of our publications for technical details.

ACCOMPLISHMENTS DURING FY 1986

Bacteriorhodopsin

Bacteriorhodopsin (bR) is a light-driven energy converter (proton pump) in the purple membrane of *Halobacterium halobium*. The removal of divalent cations converts the purple species to a blue species, profoundly affecting the normal photocycle and abolishing proton translocation by the protein. Using visible and electron spin resonance (ESR) spectroscopy, it was found that cation binding governs the conformation, and that lipid partitioning probes which decrease the negative surface charge can be added to regenerate some of the native properties. Both buried and external carboxyl residues were shown to be involved in cation binding by chemical modifications. Carboxyl groups were shown not to participate in the initial photocycle events by charge movement studies; this is unlike tyrosine groups, which effect proton entry into the conductive path.[1-3]

Thiobacillus ferroxidans

Investigation of the chemolithotrophe *Thiobacillus ferrooxidans*, an organism that utilizes iron oxidation as a means of energy generation, by low-temperature electron paramagnetic resonance (EPR) spectroscopy, resolved a new component in the electron transport chain. Characterization of the new electron carrier showed it to contain an unusual iron-sulfur cluster (Fe-S), denoted as 3FexS, as its catalytic center. Furthermore, the redox characteristics of the 3FexS cluster, in relation to other electron carriers (such as Rusticyanin), determined its position as the first step in the electron transport chain. As such, we have been able to assign the 3FexS cluster as the prosthetic group of the iron-oxidase, the primary electron acceptor in the chemolithotrophic oxidation of ferrous iron.[4]

Succinate Dehydrogenase (SDH)

SDH, a component of the oxidative electron transport pathways of mammalian and bacterial cells, consists of two protein subunits and contains one flavin adenine dinucleotide (FAD) and three Fe-S clusters. The flavin is covalently bound to a histidine in the larger (Fp) subunit. The midpoint redox potentials of the clusters S-1, S-2, and S-3 in the bacterium *Bacillus subtilis* wild type membrane-bound enzyme were determined as +80, -240, and -25 mV respectively, and magnetic reactions between S-1 and the other clusters were observed. The midpoint redox potential of the Fe-S clusters and the magnetic interactions in the FAD-deficient mutants of SDH were indistinguishable from wild type, showing that flavin has no role in the stability or magnetic interactions of the Fe-S clusters. It is concluded that conserved amino acid residues around the histidyl-FAD are important for FAD binding; however, amino acids located more than 100 residues downstream from the histidyl in the Fp subunit can also affect flavinylation.[5]

*This work was supported by the Office of Basic Energy Sciences of the U.S. Department of Energy under Contracts No. DE-AC03-76SF00098 and DE-1G03-86ER13525, a NASA Interagency Agreement A-14563c, and the Kearny Foundation for Soil Science.

†On leave from the Department of Botany, Faculty of Agriculture, The Hebrew University of Jerusalem, Rehovot, Israel.

‡On leave from the Department of Microbiology, Center of Post-Graduate Instruction and Research, University of Goa, Panaji-Goa, India.

Cyanobacteria

Environmental Stress

Exposure of the fresh water cyanobacterium *Synechococcus* 6311 to high salinity or low temperature resulted in an elevated rate of respiration and accumulation of glycogen. These elevated rates correlated with increases in membrane bound copper, which we have shown to be an integral part of the cytochrome *c* oxidase. Preliminary results indicate that the redox-driven pH gradient is utilized for the active uptake of nitrate. However, under salt stress, the pH gradient is utilized for the expulsion of salt from the cell, limiting nitrate uptake and hence protein synthesis.[6-9]

The uptake of selenium by the cyanobacterium *Synechococcus* 6311 is highly dependent on the ambient sulfate concentrations and is a light-dependent process, similar to sulfate. Under low sulfate conditions, selenium was accumulated twenty-fold and partitioned mainly in the cell wall and cytosol. It is significant that under low Se/S ratios, cellular selenium concentrations are less than that of the medium. However, under conditions where the sulfate levels are low, this organism actively accumulates selenium and may prove to be a useful component for selenium removal from contaminated waters. The elevated respiration rates in selenium-stressed cells would certainly alter the ambient oxygen levels, an important factor when considering microelement chemistry.[10]

ESR Determinations of Bioenergetic Parameters

Internal pH values in whole cells of two cyanobacterial strains were determined by ESR between pH 6 and 9 (outside) in the light and in the dark. This method allowed the determination of both the intrathylakoid and the cytoplasmic pH.[11]

Concentrations of dissolved oxygen were monitored by following the midfield line width of a nitroxide spin probe ESR spectrum. These measurements yielded accurate data over a range of oxygen concentrations (up to 5 mM). Continuous traces of second harmonic line heights yielded similar results and proved to be advantageous for kinetic measurements, but were nonlinear and less sensitive to oxygen concentrations above 2 mM. Prolonged (>1 min.) illumination caused photooxidative damage to both photosynthesis and respiration in *Agmenellum quadruplicatum*. With the addition of an impermeable paramagnetic broadening agent, rapid transients in intracellular concentrations of dissolved oxygen could be measured.[12,13]

A series of nitroxides were tested for rates of reduction in a chemical, photochemical and two biological systems by ESR assays. In all cases, piperidine and hydropyridine nitroxides were reduced consistently more rapidly than pyrroline and pyrrolidine nitroxides. Substituents on the nitroxides also affected reduction rates, with a positive charge having a major effect. The photochemical system was used to study both reduction and re-oxidation of some of the nitroxides. Reduced piperidine and hydropyridine nitroxides were also oxidized more rapidly than the reduced pyrroline and pyrrolidine nitroxides. Reoxidation subsequent to reduction was partially inhibited by superoxide dismutase, indicating that superoxide radicals are involved in the process. The original ESR signal intensity irreversibly decreased upon oxidation, implying that there was "destruction" of the spin probe concomitant with its chemical reduction in this photochemical system. Another photochemical system, which was used for generating methyl radicals, showed that the reactivity of methyl radicals with the different nitroxides was essentially independent of nitroxide structure.[14]

Noninvasive NMR Analysis of Bioenergetic Parameters in Whole Cells

We have used ^{23}Na and ^{31}P nuclear magnetic resonance (NMR) spectroscopy to elucidate some the bioenergetic changes that occur in *Synechococcus* 6311 after a transition from growth medium (0.01M NaCl) to medium containing 0.5 M NaCl. ^{23}Na-NMR analysis showed that Na rapidly penetrates the cells under dark aerobic conditions; cells grown for several days in high-salt medium, however, re-establish a low internal sodium content, which is comparable to that of control cells.

^{31}P-NMR analysis showed that when cells are presented with 0.5 M NaCl nucleotide triphospate peaks decrease, the inorganic phospate peak increases, and the cytoplasmic pH transiently increases from 7.4 to 7.9. Pyrophosphate added to cell suspensions is hydrolyzed, apparently by an extracellular phosphatase, to inorganic phosphate. Nucleotide triphosphate levels fall as much when cells are incubated in darkness as under anoxia, indicating that both respiration and photosynthesis contribute to the maintenance of intracellular ATP levels. Cells grown in high-salt medium for several generations exhibited a pattern of ^{31}P metabolites similar to control cells, except that they produced more peaks (and more intense peaks) in the monoester phosphate region, (sugar phosphates).[15,16]

PLANNED ACTIVITIES FOR FY 1987

Cyanobacteria

Our current work on the effects of environmental stress (salinity, low temperature and selenium) on algal biochemistry indicates that the biochemical lesion resulting in elevated respiration and glycogen accumulation may result from a perturbation of nitrogen metabolism, probably at the level of uptake. To determine the exact role of stress on the biochemistry of this organism, and the mechanisms involved in adaption, several lines of investigation will be followed. Elevated respiration rates will be used as an indicator of the environmental stress conditions cited above. The role of the plasma membrane, the primary barrier to environmental factors, in this biochemical function will be of particular interest. In addition to photosynthesis, respiration, and photorespiration, the physical properties of purified plasma and thylakoid membranes will be compared. Changes in permeability to ions (sodium, potassium, nitrate, bicarbonate and protons), and changes in fluidity and lipid composition under stress conditions will be determined. This line of investigation will yield valuable information on the adaptive processes occurring during environmental stress. ESR spectroscopy will be used to determine intrathylakoid and cytoplasmic pH and the effects of various ions (specifically nitrate and bicarbonate) on these parameters. In addition, the ESR oxymetric system will be used to monitor the toxic effects of oxygen on the physiology and biochemistry of cyanobacteria.

In addition to ESR, we shall apply NMR techniques to the investigation of cellular composition and bioenergetics. Noninvasive NMR analysis of whole cells will allow determination of the dynamics of the organic osmoregulant and glycogen pools (^{13}C-NMR), and give valuable information on the energy status (AMP, ADP, ATP, and Pi levels using ^{31}P-NMR) and ionic composition (Na^+ using ^{23}Na-NMR).

Bacteriorhodopsin

The role of cations in the conformation and function of bR using ESR to probe the binding sites and accessibility of quenching agents is planned. The depth of the site and identification of participating amino acids will yield information about the proximity to and effect of cations on the retinal chromophore of bR. The role of cations in conformation will be studied by heat sensitivity, with chemical modification of tyrosines and carboxyl residues. The interdependence of surface charge and cation binding will be studied using paramagnetic amphophiles.

Succinate dehydrogenase

Bacillus subtilis succinate dehydrogenase is composed of two unequal subunits and contains covalently bound FAD and iron-sulfur clusters. It is bound to the inner side of the membrane by a *b* cytochrome. The synthesis, assembly and membrane binding of this complex enzyme onto the inner side of the bacterial enzyme is not well understood. The components of the enzyme that are essential for assembly of these prosthetic groups will be studied using selected mutant strains of *B. subtilis* missing various portions of the peptides involved in catalysis, and mutants missing the b cytochrome. Using a combination of low-temperature EPR, to determine the presence of the iron-sulfur clusters, and molecular weight analysis of truncated SDH from mutants, it will be determined which iron-sulfur cluster can be assembled prior to membrane binding. Based on the amino acid sequence inferred from the DNA sequence, there exist three conserved clusters of cysteinyl residues which are the likely binding sites for the iron-sulfur clusters. We propose to determine which of these conserved sites are the likely binding sites for iron-sulfur clusters S-1 and S-2.

REFERENCES

1. Packer, L., and Arrio, B. (1986), "Characterization of Purple Membranes Containing Bacteriorhodopsin in Reconstitute Lipid Systems," in *Proceedings of the Conference on New Technological Applications of Phospholipid Bilayers, Thin Films, and Vesicles*, Tenerife, p. 6.
2. Hrabeta-Robinson, E., and Packer, L. (1987), "The Involvement of Charged Groups in Bacteriorhodopsin in Cation Binding (abstract)," Biophysical Society Annual Meeting, New Orleans, Louisiana, February 22-26, 1987.
3. Packer, L. (1986), "Utilisation des Sondes de RPE en Bionergetique Membranaire (abstract)," Societe de Chimie Biologique, Congres de Printemps, May 26-27, 1986, Gif/Yvette, France. Plenum Press, in press.
4. Fry, I.V., Lazaroff, N., and Packer, L. (1986), "Sulfate Dependent Iron Oxidation by *Thiobacillus ferrooxidans*: Characterization of a New EPR Detectable Electron Transport Component on the Reducing Side of Rusticyanin," *Arch. Biochem. Biophys. 246*, p. 650.

5. Maguire, J.J., Magnusson, K., and Hederstedt, L. (1986), "*Bacillus subtilis* Mutant Succinate Dehydrogenase Lacking Covalently Bound Flavin: Identification of the Primary Defect and Studies on the Iron-Sulfur Clusters in Mutated and Wild-Type Enzyme," *Biochemistry 25*, p. 5202.
6. Fry, I.V., Huflejt, M., Erber, W.W.A., Peschek, G.A., and Packer, L. (1986), "The Role of Respiration During Adaptation of the Freshwater Cyanobacterium *Synechococcus* 6311 to Salinity," *Arch. Biochem. Biophys. 244*, p. 686.
7. Tel-Or, E., Huflejt, M., and Packer, L. (1986), "Hydroperoxide Metabolism in Cyanobacteria," *Arch. Biochem. Biophys. 246*, p. 396.
8. Fry, I., Hrabeta, J., D'Souza, J., and Packer, L. (1986), "Application of Photosynthetic N_2-fixing Cyanobacteria to the CELSS Program," CELSS Meeting, Toulouse, France, July 2-3, 1986.
9 Packer, L., Spath, S., Baptiste, J., Robbie, C., and Bligny, R. (1987), "^{23}Na and ^{13}P Studies of Salt Stress in the Cyanobacterium *Synechococcus* 6311," Biophysical Society Annual Meeting, New Orleans, Louisiana, February 22-26, 1987.
10. Packer, L., Fry, I.V., Hrabeta, J., and Giauque, R. (1986), "Utilization of Blue Green Algae (Cyanobacteria) to Cleanse and Remove Selenium as an Option to Deal with the Problem of Salinity and Drainage in the West Side of the San Joaquin Valley," 1985-1986 Technical Progress Report, U.C. Salinity/Drainage Task Force, Division of Agriculture and Water Resources, University of California, p. 161.
11. Belkin, S., Mehlhorn, R.J., and Packer, L. (1987), "Proton Gradients in Intact Cyanobacteria," *Plant Physiology*, in press.
12. Belkin, S. and Packer, L. (1987), "Determination of Dissolved Oxygen in Photosynthetic Systems and Protective Strategies Against Its Toxic Effects in Cyanobacteria," in press.
13. Belkin, S., Mehlhorn, R.J., and Packer, L. (1987), "Determination of Dissolved Oxygen in Photosynthetic Systems by Nitroxide Spin-Probe Broadening," *Arch. Biochem. Biophys.*, in press.
14. Belkin, S., Mehlhorn, R.J., Hideg, K., Hankovsky, O., and Packer, L. (1987), "Reduction and Destruction Rates of Nitroxides," submitted to *Arch. Biochem. Biophys.*
15. Tel-Or, E., Spath, S., Packer, L. and Mehlhorn, R.J. (1987), "C-13 NMR Studies of Salt Shock-Induced Carbohydrate Turnover in the Marine Cyanobacterium *Agmenellum quadruplicatum*," *Plant Physiology*, in press.
16. Spath, L., Martin, J. Roby, C., and Bligny, R. (1987), "^{23}Na and ^{31}P NMR Studies of the Effect of Salt Stress on the Freshwater Cyanobacterium *Synechococcus* 6311," submitted for publication.

Impacts of Large Extraterrestrial Bodies and Mass Extinctions*

F. Asaro, H.V. Michel, W. Alvarez, and L.W. Alvarez

ACCOMPLISHMENTS DURING FY 1986

The Iridium Coincidence Spectrometer (ICS) has been completed for operation in a semi-automatic mode and can measure iridium content of geological samples in the parts-per-trillion (ppt) range about 500 times faster than previously possible without labor-intensive chemical separations.

In collaboration with Mark H. Anders of the Department of Geology and Geophysics of U.C. Berkeley, a nearly continuous sampling covering over 250 meters (the last 14 million years) of sediment has been made of highly calcareous ooze from a DSDP core Hole 588B from the Southwest Pacific Ocean.

Using the ICS for 7-minute counts in the manual mode after irradiation with 1.2×10^{-19} neutrons/cm^2 at the University of Missouri Triga Research reactor, a single Ir peak with 155 ppt Ir was found in ~33 meters of sediment deposited over about 2.7 million years (MY)[1]. The average background was ~11 ppt, and additional longer counting times were used to better define the Ir anomaly with a precision of ~1-2 ppt Ir. The Ir anomaly is not caused by changes in the sedimentation of $CaCO_3$. Such a change in sedimentation rate would also cause a peak in the aluminum abundance similar to that found for Ir. As can be seen in Fig. 1, there is no aluminum peak where the Ir peak is found.

The ICS was also used to study a core taken from the sea bottom deposited 34-39 MY ago near New Zealand at ~36°38′ south latitude. A distinct Ir anomaly of 200 ppt was found exactly where it was expected based on the stratigraphic sequence found in other sites. In addition, there were two other smaller Ir peaks—one (38 ppt Ir) 30 cm below the main peak and the other (28 ppt Ir) 220 cm above. The background was low, 9 ppt Ir, with no detectable variation. The Ir in the main peak, $\sim 0.6 \times 10^{-9}$ gm/cm^2 of sediment, is in the range found for ten other sites studied.

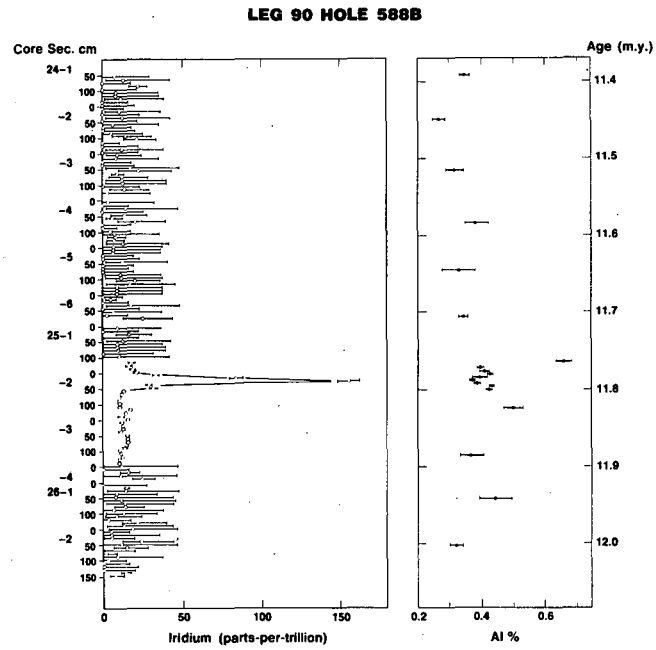

Figure 1. Ir anomaly in 11.8 million year old sediments from DSDP Leg 90 Hole 588B from the Southwest Pacific Ocean. (XBL 8612-9288).

PLANNED ACTIVITIES FOR FY 1987

Work is continuing studying the origin of the Ir and its significance to the Nemesis theory of multiple comet impacts every 26 MY.

REFERENCES

1. Alvarez, L.W., "Mass Extinctions Caused by Large Bolide Impacts," presented at the Royal Academy of Sciences, Stockholm, Sweden, December 11, 1986; LBL Report LBL-22786 (1987).

*This work was supported by the Director, Office of Energy Research, Office of Basic Energy Sciences, Engineering and Geosciences Division of the U.S. Department of Energy under Contract No. DE-AC03-76SF00098 and the National Aeronautics and Space Administration Ames Research Center under Contract No. A-71683B. Support was also received from the Murdock Charitable Trust.

LAWRENCE BERKELEY LABORATORY
TECHNICAL INFORMATION DEPARTMENT
UNIVERSITY OF CALIFORNIA
BERKELEY, CALIFORNIA 94720